Next Materials 8 (2025) 100685

Contents lists available at ScienceDirect

Next Materials

journal homepage: www.sciencedirect.com/journal/next-materials

Research article

Green synthesis of nanoparticles using cottonwood and rambutan honeys: Optimization, characterization, and enhanced antioxidant activity with reduced toxicity via oligochitosan coating

Saidun Fiddaroini [a], Friske Prisilia [a], Silvana Br Karo [a], Luailik Madaniyah [a], Almas Dwi Khairana [a], Galuh Rahmaniah [a], Suci Amalia [b], Aulanni'am [a], Moh. Farid Rahman [a], Layta Dinira [a], Qonitah Fardiyah [a], Akhmad Sabarudin [a,c,*]

[a] Department of Chemistry, Faculty of Science, Brawijaya University, Malang, Indonesia
[b] Chemistry Study Program, Faculty of Science and Technology, Maulana Malik Ibrahim Islamic State University, Malang, Indonesia
[c] Research Center for Advanced System and Material Technology, Brawijaya University, Malang, Indonesia

ARTICLE INFO

Keywords:
Silver nanoparticle
Oligochitosan
Honey
Antioxidant
Toxicity

ABSTRACT

The green synthesis of silver nanoparticles (AgNPs) using bio-based reductants has gained significant attention due to its environmentally friendly and sustainable approach. This study aims to optimize the synthesis, characterize the physicochemical properties, and evaluate the biological activities of AgNPs synthesized using cottonwood (*Ceiba pentandra*) and rambutan (*Nephelium lappaceum*) honeys as bioreducing agents, with further functionalization by oligochitosan to enhance stability and bioactivity. Comprehensive characterization using UV-Vis spectroscopy, FTIR, PSA-DLS TEM, FESEM-EDX, and XRD confirmed the formation of spherical nanoparticles with an average size of 9.01 nm. The particle size distribution followed a lognormal model with an R^2 value of 0.925, indicating high statistical reliability. The biological activities of AgNPs and AgNPs-Ch composites were evaluated through antioxidant and toxicity assays. The DPPH assay demonstrated a 3.00–3.41-fold enhancement in antioxidant activity upon chitosan coating, suggesting a synergistic interaction between AgNPs and oligochitosan in free radical scavenging. Furthermore, toxicity assessment using *Artemia salina* nauplii revealed a substantial 6.12–6.19-fold reduction in toxicity for AgNPs-Ch compared to uncoated AgNPs, highlighting the protective role of chitosan in mitigating silver ion release. These findings underscore the potential of honey-derived AgNPs and their chitosan composites for biomedical and environmental applications, providing a sustainable route for nanoparticle synthesis with improved biofunctionality and safety.

1. Introduction

Nanotechnology has revolutionized various scientific fields, including medicine [1], environmental science [2,3], and materials engineering [1,4], through the development of nanoparticles with tailored properties. Among these, AgNPs have garnered significant attention due to their exceptional physicochemical characteristics, including high surface area [5–7], unique optical properties [8,9], and remarkable antimicrobial [10,11] and antioxidant activities [12,13]. AgNPs are widely utilized in various scientific fields, making the optimization of their synthesis a critical area of research.

The synthesis of AgNPs using environmentally friendly approaches, such as green chemistry, has emerged as a sustainable alternative to conventional chemical and physical methods [14,15]. In particular, the use of natural reductants, such as plant extracts [16–18], fungi [19,20], and honey [11,21], has gained momentum due to their non-toxic nature and reduced environmental impact [22,23]. Honey, a naturally occurring bioreductant, is rich in polyphenols, flavonoids, and reducing sugars [24,25], which facilitate the reduction of silver ions and the stabilization of nanoparticles [26,27]. However, achieving consistent and optimized synthesis of AgNPs with desirable characteristics remains a challenge due to variations in the chemical composition of natural reductants [11].

Optimization of the synthesis process plays a crucial role in controlling the physicochemical properties of AgNPs, including particle size, morphology, and stability, which in turn influence their biological

* Corresponding author at: Department of Chemistry, Faculty of Science, Brawijaya University, Malang, Indonesia.
E-mail address: sabarjpn@ub.ac.id (A. Sabarudin).

https://doi.org/10.1016/j.nxmate.2025.100685
Received 12 February 2025; Received in revised form 9 April 2025; Accepted 24 April 2025
Available online 28 April 2025

activities [28]. Key synthesis parameters such as reaction duration, bioreductant concentration, and silver precursor concentration significantly impact nanoparticle formation. Reaction duration affects the growth and nucleation rate of AgNPs, where shorter durations may lead to incomplete reduction, resulting in larger and polydisperse nanoparticles, while excessive reaction times may lead to unnecessary aggregation [6,29–31]. Similarly, the concentration of the bioreductor determines the availability of reducing agents and stabilizing compounds; an optimal concentration is essential to achieve a balance between reduction efficiency and nanoparticle stabilization [32,33]. Furthermore, silver precursor concentration is a crucial factor that dictates the density of available silver ions for nucleation and growth. An excessive concentration of silver ions can lead to uncontrolled growth and aggregation, whereas insufficient silver content may hinder effective nanoparticle formation [34].

Irradiation serves as a catalytic driver in the synthesis of AgNPs by accelerating the reduction of Ag^{+} ions to elemental silver (Ag^{0}). Various irradiation sources, including UV light [35], visible light [36], and microwave radiation [37], have been employed to regulate particle size, distribution, and stability. The underlying mechanism is governed by photon energy absorption by either the precursor or the reducing agent, directly influencing nucleation kinetics and nanoparticle growth [38]. The choice of irradiation type plays a critical role in tailoring the physicochemical properties of AgNPs, making it a key parameter for optimizing their functionality in specific applications.

In addition to their synthesis, the biological activities of AgNPs, including antioxidant and toxicity properties, are critical for evaluating their applicability in various fields. The incorporation of biopolymers, such as oligochitosan, into AgNPs has been reported to enhance their stability and biological performance [17,39]. The antioxidant potential of AgNPs and their composites can be evaluated using assays like DPPH, which provide insights into their free radical scavenging capabilities [40,41]. Furthermore, toxicity assessment using model organisms, such as *Artemia salina* nauplii, offers a reliable method for determining their biocompatibility and safety for future applications [42,43]. The interplay between synthesis conditions and biological properties underscores the need for systematic optimization to maximize the efficacy and applicability of AgNPs-based materials [44].

This study aims to optimize the synthesis of AgNPs using honey as a green reducing agent and evaluate the antioxidant and toxicity properties of AgNPs and their chitosan composites. The synthesis optimization is conducted by varying Ag concentration, bioreductor concentration, and exposure duration. Additionally, sunlight irradiation is selectively filtered using plastic filters to identify the optimal wavelength (visible light) most influential in sunlight for AgNPs synthesis. Once the optimal conditions for each honey type are determined, AgNPs are further modified with oligochitosan coating to enhance biocompatibility. The characterization of AgNPs in this study encompasses a comprehensive suite of analytical techniques. UV-Vis spectroscopy is employed to assess the surface plasmon resonance of AgNPs, providing insights into their optical properties and formation dynamics. FTIR spectroscopy is utilized to elucidate molecular interactions and chemical transformations occurring during synthesis and oligochitosan coating. Morphological and compositional analyses are conducted using TEM and FESEM-EDX, enabling high-resolution visualization and elemental mapping of AgNPs. Stability assessments post-coating are performed via PSA-DLS to evaluate hydrodynamic size distribution and colloidal stability. Furthermore, XRD analysis is conducted to determine the crystallite structure of AgNPs before and after oligochitosan functionalization, offering critical insights into phase composition and structural integrity.

Through a systematic analysis of synthesis parameters and the integration of advanced characterization techniques, this study provides a comprehensive understanding of the relationship between synthesis conditions, physicochemical properties, and biological activity of AgNPs. The findings offer valuable insights into the design and application of AgNPs-based materials in biomedicine and environmental science, supporting the development of nanoparticles with enhanced functionality and controlled biocompatibility.

2. Material and method

2.1. Materials and instrumentation

The chemicals used in this research were silver nitrate ($AgNO_3$, EMSURE 99 %), low-molecular-weight (LMW) chitosan (deacetylation degree 75 %–85 %; 50–190 kDa; SIGMA-ALDRICH), glacial acetic acid (CH_3COOH; 99 % EMSURE), hydrogen peroxide (H_2O_2, 30 % SMART-LAB), Ethanol (C_2H_6O, Smartlab; Absolute 98 %), and 2,2-diphenyl-1-picrylhydrazyl (DPPH; SIGMA-ALDRICH). Additionally, this study utilized various bioreductors, specifically cottonwood (*Ceiba pentandra*) honey and rambutan (*Nephelium lappaceum*) honey. all sourced from Tawon Rimba Raya Farm in Malang, East Java, Indonesia. The instruments used were UV–Vis (Shimadzu 1601 Series), FTIR (Shimadzu 8400 s), PSA-DLS (Malvern Panalytical, UK), FESEM-EDX (FEI - Quanta FEG 650), and XRD (PANalyticaln X'Pert PRO).

2.2. Synthesis of AgNPs

AgNPs were synthesized by combining honey at varying concentrations (0.75 %, 1.5 %, and 3 %) with silver nitrate ($AgNO_3$) solutions at different concentrations (0.025 M, 0.05 M, and 0.1 M) in equal volumes. The mixtures were thoroughly stirred using a magnetic stirrer for 10 minutes at room temperature (26 °C–30 °C). After homogenization, the solutions were exposed to sunlight (intensity range: 88,400–137,600 lux; temperature range: 26 °C–34 °C) for 10 minutes. The formation of AgNPs was indicated by a distinct color change from colorless to brown. This process was repeated for each type of honey tested.

The effect of wavelength exposure on AgNPs synthesis was examined using honey that exhibited the most notable color change. Sunlight wavelengths corresponding to the visible spectrum (red, yellow, green, blue, and violet) were filtered using colored plastic films. The transmitted wavelengths were measured with a spectrometer apps in mobile phone, and their influence on the synthesis process was evaluated through UV-Vis spectrophotometry. The key optimization parameters for the synthesis process are summarized in Table 1.

This method follows a green synthesis approach, utilizing natural bioreductor from honey and a natural catalyst in the form of sunlight, making it an eco-friendly and sustainable alternative to conventional nanoparticle synthesis methods.

2.3. Oligochitosan coating on AgNPs

The coating of AgNPs with oligochitosan involves an initial depolymerization and deacetylation process using low molecular weight chitosan to produce oligochitosan, following the protocol established in our previous study [11]. Oligochitosan (water-soluble chitosan) was prepared by dissolving 0.4 g of LMW chitosan in 20 mL of 1 % acetic acid and stirring for 2 hours. Depolymerization was performed by adding 10 % H_2O_2 up to 20 mL and stirring for another 2 hours. The solution was then neutralized to pH 7 using 10 % NaOH, filtered, and the filtrate was collected as oligochitosan.

AgNPs with the optimal characteristics from each honey type (cottonwood and rambutan) are then modified by mixing with oligochitosan in a 1:1 vol ratio. The coating process is conducted by gradually adding AgNPs into the oligochitosan solution under continuous stirring at 250 rpm at room temperature (27–30°C). This controlled mixing results in the formation of oligochitosan-coated AgNPs (AgNPs-Ch), appearing as a clear solution.

Table 1
Optimization parameters of AgNPs synthesis.

Parameter Optimization	Exposure Duration	Honey Concentration	$AgNO_3$ Concentration	Type of Exposure
Exposure Duration	5 min	3 %	0.05 M	Sunlight
	10 min	3 %	0.05 M	Sunlight
	15 min	3 %	0.05 M	Sunlight
	20 min	3 %	0.05 M	Sunlight
Honey Concentration	10 min	3 %	0.05 M	Sunlight
	10 min	1.5 %	0.05 M	Sunlight
	10 min	0.75 %	0.05 M	Sunlight
$AgNO_3$ Concentration	10 min	3 %	0.1 M	Sunlight
	10 min	3 %	0.05 M	Sunlight
	10 min	3 %	0.025 M	Sunlight
Type of Exposure	10 min	3 %	0.05 M	Sunlight-Red filter
	10 min	3 %	0.05 M	Sunlight-Yellow filter
	10 min	3 %	0.05 M	Sunlight-Green filter
	10 min	3 %	0.05 M	Sunlight-Blue filter
	10 min	3 %	0.05 M	Sunlight-Purple filter

2.4. Characterizations

2.4.1. UV-Vis spectroscopy

UV-Vis spectroscopy was utilized to investigate the formation of AgNPs synthesized using honey as a natural reductant. Spectral measurements were performed using a UV-Vis spectrophotometer across the wavelength range of 200–800 nm. The AgNPs samples were analyzed in 1 cm quartz cuvettes, and the absorbance was recorded at the characteristic maximum wavelength (λmax) of AgNPs, typically observed between 400 and 450 nm. The presence of absorbance peaks in this region confirmed the successful synthesis of AgNPs, attributed to surface plasmon resonance phenomena.

Furthermore, UV-Vis spectroscopy was employed to evaluate the optical properties of oligochitosan and AgNPs-Ch composites. The addition of oligochitosan to AgNPs induced a shift and alteration in the absorbance peak within the 400–450 nm range, indicative of molecular interactions between AgNPs and oligochitosan. This spectral shift corroborated the successful formation of a stable AgNPs-Chitosan complex, demonstrating the effective incorporation of chitosan into the AgNPs matrix and highlighting its potential for enhanced stability and functionality.

2.4.2. Transmission electron microscopy

The morphological characterization and particle size distribution analysis of AgNPs were conducted utilizing TEM with a JEM-1400 instrument (JEOL, Japan). Prior to imaging, the colloidal AgNPs sample was prepared by depositing 1–2 μL of the colloidal solution onto a carbon-coated copper grid (300 mesh), followed by air-drying at room temperature to remove residual solvents.

TEM imaging was performed at an accelerating voltage of 120 kV, with a magnification of 150,000 × , to obtain high-resolution images enabling detailed morphological and size distribution analysis. Particle size measurements were conducted using ImageJ software, where more than 100 nanoparticles were analyzed to generate a statistically representative size distribution. Subsequently, a histogram was constructed, and the particle size distribution was evaluated using a lognormal model, with statistical parameters including mean particle size and standard deviation being determined.

2.4.3. Fourier transform infra-red

FTIR spectroscopy was utilized to analyze the chemical composition and molecular interactions present in honey, AgNPs, oligochitosan, and AgNPs-Ch composites. For honey, FTIR analysis was performed directly in its liquid state without any additional preparation, as freeze-drying was unnecessary. Conversely, the AgNPs, oligochitosan, and AgNPs-Ch samples were subjected to freeze-drying prior to analysis. This step concentrated the materials, enhancing measurement precision and reducing interference from solvents. FTIR spectroscopy was employed to detect changes in functional groups and molecular interactions, such as the reduction of silver ions by honey and the formation of AgNPs-Chitosan complexes. The measurements were conducted at room temperature, covering a wavenumber range of 400–4000 cm^{-1} .

2.4.4. Particle size analyzer - dynamic light scattering

The hydrodynamic size distribution and colloidal stability of AgNPs and AgNPs-Ch were characterized using a Zetasizer Advance Series (Malvern Panalytical, UK) based on Dynamic Light Scattering (DLS) and Electrophoretic Light Scattering (ELS) techniques. Samples were dispersed in deionized water and sonicated to prevent aggregation before measurement.

Particle size distribution was analyzed at 25°C using a He-Ne laser (633 nm, 10 mW) and a backscattering detection angle of 173°, ensuring high sensitivity for nanoscale measurements. The Z-average diameter and polydispersity index (PI) were determined through cumulant analysis, where a PI < 0.3 indicated a monodisperse system.

Zeta potential was measured using an electrophoretic mobility mode with a universal dip cell to assess surface charge and colloidal stability. Values within $\pm$ 30 mV were considered indicative of stable dispersions due to sufficient electrostatic repulsion. Data processing was performed using Zetasizer Software 8.01 to obtain size distribution profiles and stability parameters.

2.4.5. X-ray diffraction

The crystallite structure of oligochitosan, AgNPs, and AgNPs-Ch was analyzed using XRD. Sample preparation involved freeze-drying the materials to obtain dry powder suitable for XRD analysis. The measurements were performed on AgNPs exhibiting optimal characteristics as determined by prior UV-Vis and FTIR analyses. XRD data acquisition was conducted using a diffractometer equipped with a Cu-Kα radiation source ($\lambda = 1.5406$ Å) operating at 30 mA and 40 kV. The scan range was set between 10.0084° and 89.9764° (2θ) with a step size of 0.0170° and a scan time of 10.160 seconds per step. A continuous scanning mode was employed, with fixed divergence slit settings at 0.8709°. The goniometer radius was maintained at 240 mm, and the distance of the focus-divergence slit was 100 mm. During the analysis, the sample was positioned with a specimen length of 10 mm and analyzed at a constant temperature of 25 °C.

2.4.6. Field emission scanning electron microscopy - energy dispersive X-ray spectroscopy

The morphological and elemental characterization of oligochitosan, AgNPs, and AgNPs-Ch was performed using Field Emission Scanning Electron Microscopy (FESEM) coupled with Energy Dispersive X-ray Spectroscopy (EDS). Samples were prepared by depositing each material onto silicon (Si) wafers to form uniform thin films. Oligochitosan was prepared as a dry powder or thin film from its aqueous solution, AgNPs

were deposited directly from the optimized colloidal suspension, and AgNPs-Ch composites were formed by drying the mixture of AgNPs and oligochitosan onto the substrate.

The analyses were conducted using an FEI Quanta FEG 650 FESEM equipped with an Oxford Instrument X-act EDS detector and AZtecOne software. The system operated in high-vacuum mode with an accelerating voltage of 20 kV, a spot size of 5, a dwell time of 1 μs, and a working distance of 10 mm. Backscattered electron (BSE) imaging was employed at a magnification of 50,000 × to observe the surface morphology of the samples. EDS measurements were conducted on specific regions of the samples to determine their elemental composition and confirm the presence of key elements in each sample. The FESEM imaging provided detailed insights into the surface morphology, while EDS spectra were used to determine the chemical composition. FESEM-EDX analysis was performed on AgNP samples exhibiting optimal characteristics, as determined by prior UV-Vis and FTIR analyses.

2.5. In vitro antioxidant activity

The antioxidant activity of honey, AgNPs, oligochitosan, and AgNPs-Ch composites was assessed using the DPPH (2,2-diphenyl-1-picrylhydrazyl) radical scavenging assay. For each sample, various concentrations were prepared in methanol to evaluate their ability to neutralize DPPH free radicals. A methanolic solution of DPPH (0.1 mM) was freshly prepared and used as the radical source. In a typical experiment, 1 mL of DPPH solution was mixed with 1 mL of each sample solution at the desired concentration. The mixture was incubated in the dark at room temperature for 30 minutes to allow the reaction to proceed.

The absorbance of the reaction mixture was measured at 517 nm using a UV-Vis spectrophotometer, with methanol as the blank. The percentage of DPPH radical inhibition was calculated using the **Equation 1**:

$$\%\text{Inhibition} = \frac{A\ \ (control) - A\ \ (sample)}{A\ \ (control)} \times 100\% \quad (1)$$

Where A (control) is the absorbance of the DPPH solution without the sample, and A (sample) is the absorbance of the DPPH solution with the sample. Each test was performed in triplicate to ensure reproducibility, and the results were expressed as the percentage of DPPH radical scavenging activity. The antioxidant activity was analyzed across a range of concentrations to determine the dose-dependent efficacy of each sample. Honey and oligochitosan were tested independently, while AgNPs and AgNPs-Ch composites synthesized using cottonwood and rambutan honey were evaluated to assess the role of honey type and chitosan coating on their antioxidant performance.

2.6. In vivo toxicity test

The *in vivo* toxicity evaluation of AgNPs and AgNPs-Ch composites was conducted using the Brine Shrimp Lethality Assay (BSLA) in accordance with ethical clearance No. 177-KEP-UB-2024. This assay involved exposing Artemia salina nauplii to varying concentrations of the test samples to assess their toxicological impact. For each test, 10 nauplii were introduced into individual sample solutions prepared at different concentrations. The samples were incubated for 24 hours, and the survival of nauplii was subsequently monitored. Nauplii were classified as dead if they exhibited no active forward motion during a 30-second observation period under controlled conditions. The numbers of surviving and deceased nauplii in each sample were recorded, and the percentage mortality was determined using the **Equation 2**:

$$\%\text{Mortality} = \frac{Number\ of\ dead\ nauplii}{Total\ nauplii(dead + alive)} \times \quad 100 \quad (2)$$

The mortality data were analyzed to calculate the LC_{50} value, defined as the concentration of the test sample required to induce 50 % mortality in the nauplii population. The LC_{50} value served as a critical parameter for assessing the relative toxicity of each sample, enabling a quantitative comparison of toxicity levels between AgNPs and AgNPs-Ch composites. This analysis provided valuable insights into the biocompatibility and potential environmental impact of the synthesized nanomaterials.

3. Result and discussions

3.1. Synthesis of AgNPs

The synthesis of AgNPs using honey as a bioreducing agent represents a green and eco-friendly approach, leveraging the natural components of honey to reduce silver ions (Ag^+) from silver nitrate ($AgNO_3$) to elemental silver (Ag^o). Honey, rich in organic compounds such as reducing sugars (glucose and fructose), plays a dual role as both a reducing agent and a natural stabilizer. The reduction of silver ions is initiated through the oxidation of aldehyde groups in reducing sugars, where electrons are donated to Ag^+, transforming it into elemental silver (Ag^o). This reduction process can be accelerated by exposure to heat or sunlight, which acts as an energy source to facilitate the reaction. For instance, glucose in honey undergoes oxidation to form gluconic acid, while Ag^+ ions are reduced to Ag^o, initiating the nucleation of silver nanoparticle seeds.

The mechanism underlying AgNPs formation involves the crucial participation of reducing sugars, such as glucose and fructose, which play a central role in the reduction process (Fig. 1). The chemical structure of these sugars contains reactive functional groups—hydroxyl (-OH) and aldehyde (-CHO) in glucose, and ketone in fructose—prone to oxidation. These groups interact with silver ions, reducing Ag^+ to Ag^o. In the early stages, the aldehyde groups in glucose and the ketone groups in fructose are oxidized, forming carboxyl groups while Ag^+ ions are reduced to silver atoms (Ag^o). This reduction initiates the formation of small silver nanoparticle seeds, a critical step known as nucleation.

During nucleation, individual Ag^o atoms aggregate to form small clusters or nuclei, which serve as the initial seeds for further particle growth. This stage is crucial for achieving uniform nanoparticle size distribution. Following nucleation, the growth phase begins, where these nuclei coalesce into larger nanoparticles. The size and morphology of the resulting nanoparticles are strongly influenced by various reaction parameters, such as temperature, reactant concentration, and reaction time. Typically, the resulting AgNPs are spherical or near-spherical in shape, although other morphologies may arise depending on the specific reaction conditions.

The stabilization of AgNPs is achieved through the presence of organic compounds in honey, such as phenolic acids and flavonoids, which adsorb onto the nanoparticle surface. This adsorption forms a protective layer, preventing further growth and aggregation while ensuring long-term stability in solution. This step is essential for maintaining nanoparticle dispersion and preserving their functionality. Beyond serving as reducing agents, the organic constituents in honey also play a vital role in stabilizing the nanoparticles.

Biosynthesis of AgNPs using honey provides a straightforward, sustainable, and economical method to produce silver nanoparticles. The reducing sugars in honey drive the conversion of Ag^+ ions to Ag^o, while its bioactive compounds stabilize the resulting nanoparticles. This green approach aligns with sustainable chemistry principles and offers considerable potential in biomedical applications, including as antibacterial agents, antioxidants, and anticancer therapies. Moreover, by adjusting reaction parameters, the size and morphology of AgNPs can be precisely controlled, enabling the creation of nanoparticles with tailored properties for specific applications.

Honey's natural composition, rich in reducing sugars, phenolic compounds, and antioxidants, presents significant advantages over other bioreductors. It simplifies the synthesis process by eliminating the need for complex extraction steps, as it can be directly mixed into the

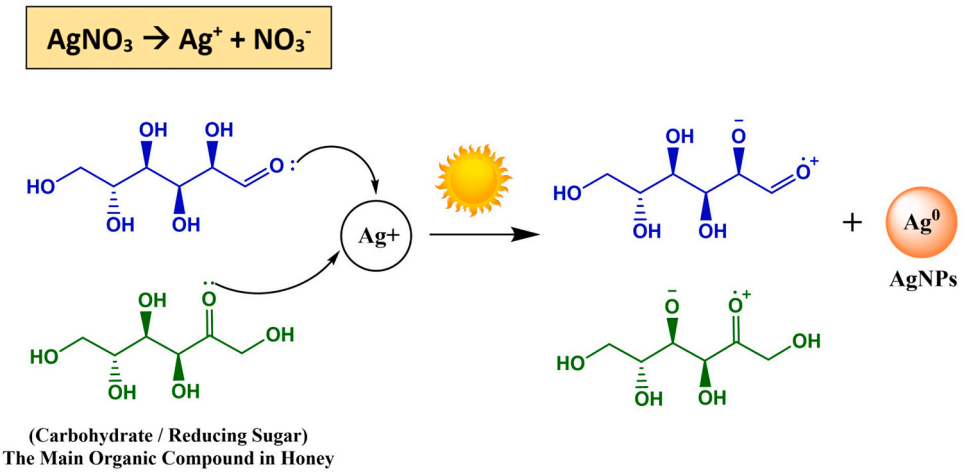

Fig. 1. Mechanism of AgNPs Formation by Honey Bioreductor.

reaction solution. This straightforward preparation not only reduces time and costs but also preserves its bioactive components, supporting a more sustainable and efficient synthesis method.

3.2. Optimizations of AgNPs synthesis

The UV-Vis spectra presented in both panels illustrate the formation of AgNPs reduced by Cottonwood honey (AgNPs Cottonwood) and Rambutan honey (AgNPs Rambutan), respectively, under varying sunlight exposure times (Fig. 2). The absorption peaks observed in these spectra offer critical insights into the optimization of exposure duration and wavelength for efficient AgNPs synthesis, a process primarily driven by the surface plasmon resonance (SPR) phenomenon. SPR peaks, which typically occur between 400 and 450 nm for AgNPs, are indicative of the collective oscillation of conduction band electrons in response to light, reflecting the size, shape, and concentration of the nanoparticles.

In the spectra derived from AgNPs Cottonwood (Fig. 2**a**), an observable increase in absorbance occurs as the sunlight exposure time is extended from 5 to 20 minutes. The SPR peak appears consistently around 420–450 nm, with the highest absorbance recorded at 20 minutes of exposure. This progressive increase in absorbance intensity indicates a time-dependent enhancement in the quantity of AgNPs formed. The distinct change in solution color from yellow to deep red further corroborates this finding, as it signifies the transition from smaller AgNPs to larger and more concentrated nanoparticle formations. Therefore, a 20-minute exposure duration emerges as the optimal condition for maximizing nanoparticle yield and size based on the peak SPR intensity. The formation of nanoparticles with greater absorbance reflects a higher concentration of colloidal AgNPs in the solution, which is driven by the extended exposure time allowing more complete reduction of silver ions (Ag^+) to elemental silver (Ag^0).

For AgNPs Rambutan (Fig. 2**b**), a similar trend is observed, with increasing sunlight exposure time leading to a gradual enhancement in absorbance intensity at the SPR peak (~420 nm). However, it is important to note that the overall absorbance values for Rambutan honey are lower compared to Cottonwood honey, even at the maximum exposure time of 20 minutes. This suggests that while Rambutan honey is capable of reducing Ag^+ to Ag^0, it may do so less efficiently than Cottonwood honey, potentially due to differences in the composition of reducing sugars, phenolic compounds, or other organic constituents. The relatively lower absorbance intensities imply that fewer AgNPs are formed, or that the nanoparticles are smaller in size or lower in concentration. Nevertheless, the observed color change in the Rambutan honey solutions (from yellow to red) confirms the successful synthesis of

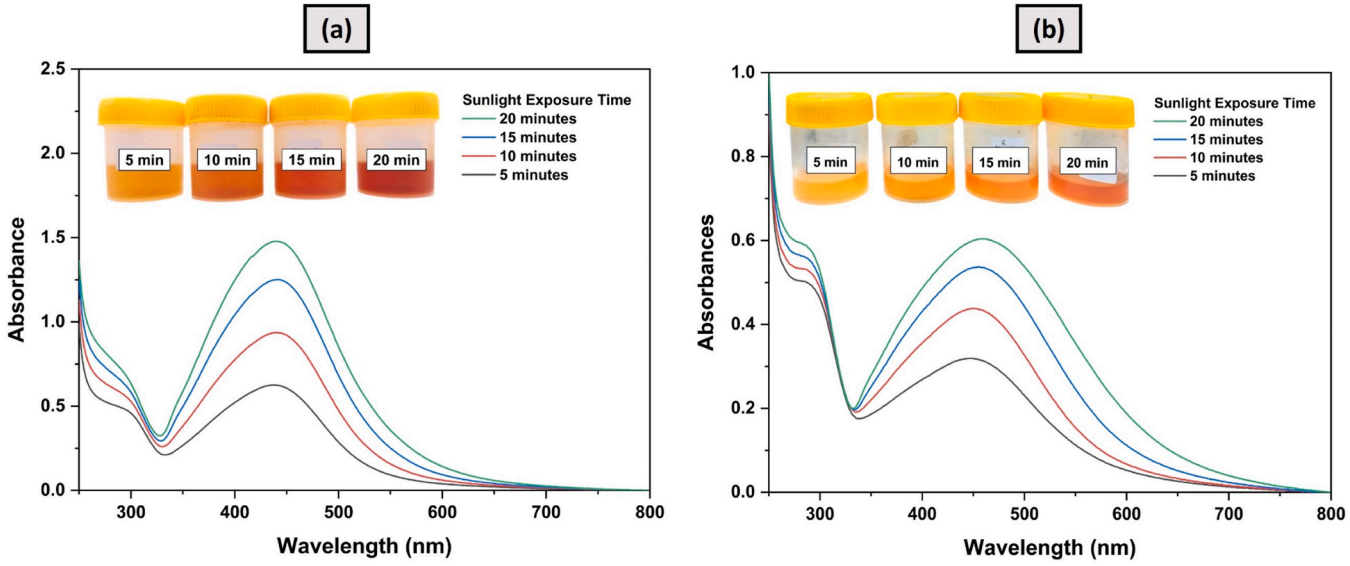

Fig. 2. The effect of sunlight exposure duration on the synthesis of AgNPs Cottonwood (a), and AgNPs Rambutan (b).

AgNPs, albeit at a slower or less efficient rate than with Cottonwood honey.

The effect of sunlight exposure time is the gradual increase in absorbance with time indicates that prolonged sunlight exposure not only accelerates the reduction process but also promotes nanoparticle growth through the coalescence of smaller Ag^{o} nuclei. While extended exposure generally favors the formation of larger or more concentrated nanoparticles, it is essential to optimize this duration to prevent excessive particle growth or aggregation, which could diminish the functional properties of the AgNPs. The results suggest that while both honeys can be used for green synthesis, Cottonwood honey offers greater potential for producing AgNPs with higher yields and possibly more favorable size distributions due to its higher reducing power.

The UV-Vis spectra for both Cottonwood and Rambutan honey demonstrate that sunlight exposure significantly influences the formation and characteristics of AgNPs. A 20-minute exposure duration is optimal for achieving maximal nanoparticle formation in both cases, with Cottonwood honey showing superior performance in terms of AgNPs yield and concentration. This difference underscores the importance of selecting an appropriate bioreductant based on its inherent reducing capacity and composition. Despite the 20-minute sunlight exposure producing a darker AgNPs solution, indicating larger particle sizes due to extended growth and aggregation, it also reflects a higher concentration and more substantial formation of AgNPs. However, the antibacterial activity tends to decrease when nanoparticle sizes are larger or aggregated. Larger particles reduce the surface area available for interaction with bacterial cells, thereby diminishing the overall effectiveness of the AgNPs. Therefore, for future optimizations, a 10-minute exposure duration is preferable, as it results in a more stable AgNPs product with smaller particle sizes, enhancing its antibacterial activity while maintaining adequate nanoparticle formation.

Based on the UV-Vis spectra, the results depicted in Fig. 3**a**, which illustrates the reduction of AgNPs using Cottonwood honey, show that an $AgNO_3$ precursor concentration of 0.05 M yields optimal results. This is evidenced by the higher absorbance intensity compared to concentrations of 0.025 M and 0.1 M, as well as a distinct and well-defined localized surface plasmon resonance (LSPR) peak around 400–450 nm. The 0.05 M concentration strikes a balance between the sufficient availability of Ag^{+} ions for reduction into AgNPs and the reducing activity of the bioactive compounds in randu honey. At the 0.025 M concentration, the limited availability of Ag^{+} ions results in a relatively smaller quantity of AgNPs, as reflected by lower absorbance. On the other hand, at 0.1 M, although the Ag^{+} concentration increases, the reducing compounds in randu honey may be less effective in stabilizing the nanoparticles due to aggregation or the formation of excessively large particles, leading to no significant increase in absorbance intensity.

In contrast, Fig. 3**b** representing the reduction of AgNPs using rambutan honey, indicates that the concentration of $AgNO_3$ does not have a significant impact on either the absorbance intensity or the position of the LSPR peak. This suggests that the bioactive compounds in rambutan honey, such as flavonoids, phenolics, or enzymes, may exhibit lower reducing and stabilizing capacities compared to randu honey. As a result, regardless of the $AgNO_3$ concentration, the amount of nanoparticles formed remains relatively uniform, and the LSPR peak is consistently positioned in a similar region.

Therefore, the results demonstrate that Cottonwood honey is more sensitive to variations in $AgNO_3$ precursor concentration, with an optimal concentration at 0.05 M, whereas rambutan honey shows more stable performance and is less affected by changes in $AgNO_3$ concentration.

The UV-Vis spectra presented illustrate the influence of honey concentration on the formation of AgNPs Cottonwood (Fig. 4**a**) and AgNPs Rambutan (Fig. 4**b**). The characteristic surface plasmon resonance (SPR) peak of AgNPs is observed within the wavelength range of 400–450 nm, confirming successful nanoparticle formation. In both cases, increasing the honey concentration from 0.75 % to 3 % results in a pronounced enhancement in SPR peak intensity. This trend indicates that higher honey concentrations facilitate more efficient reduction of silver ions (Ag^{+}) to AgNPs. The bioactive compounds in honey, including flavonoids, phenolics, and enzymes, act as reducing and stabilizing agents. A higher honey concentration provides an increased abundance of these active molecules, enabling the formation of a larger quantity of nanoparticles or nanoparticles with more uniform sizes, as evidenced by the elevated SPR intensity.

Comparatively, the spectra reveal that cottonwood honey (Fig. 4**a**) generates higher SPR intensities than rambutan honey (Fig. 4**b**) at equivalent concentrations. This suggests that cottonwood honey contains a greater concentration or higher efficiency of bioactive compounds in reducing silver ions and stabilizing the resulting nanoparticles. Additionally, the variation in solution color with increasing honey concentration further supports differences in nanoparticle size, distribution, and concentration. These variations are likely due to the distinct chemical compositions inherent to each honey type.

Overall, increasing honey concentration enhances the efficiency of

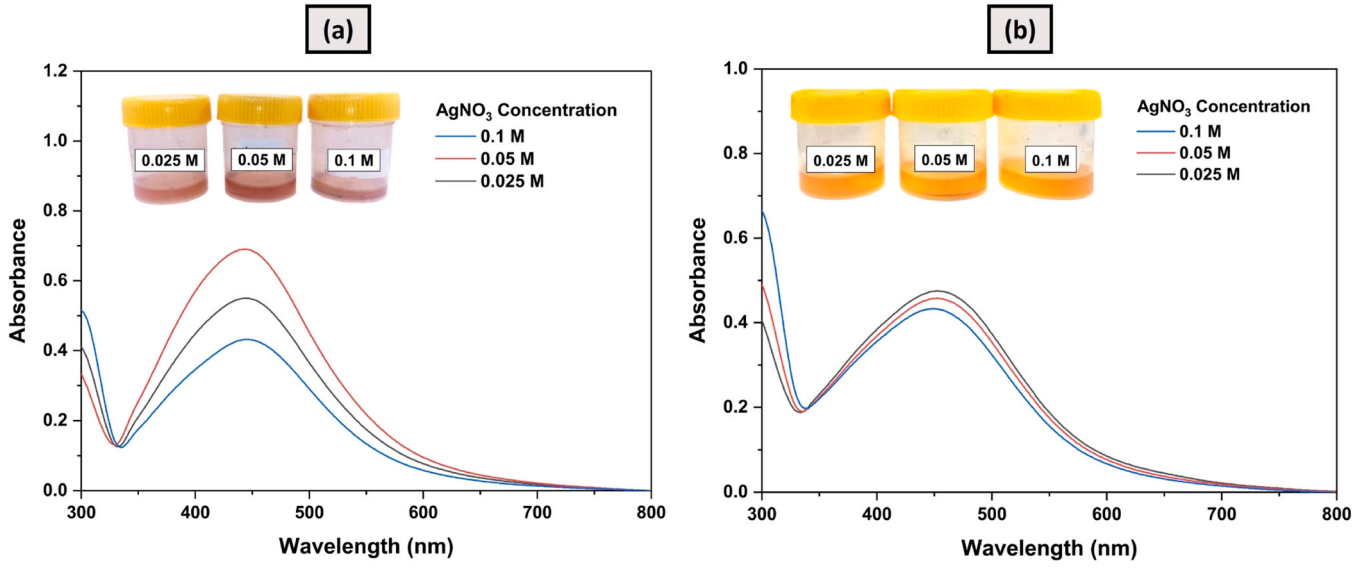

Fig. 3. The effect of $AgNO_3$ Concentration on the synthesis of of AgNPs Cottonwood (a), and AgNPs Rambutan (b).

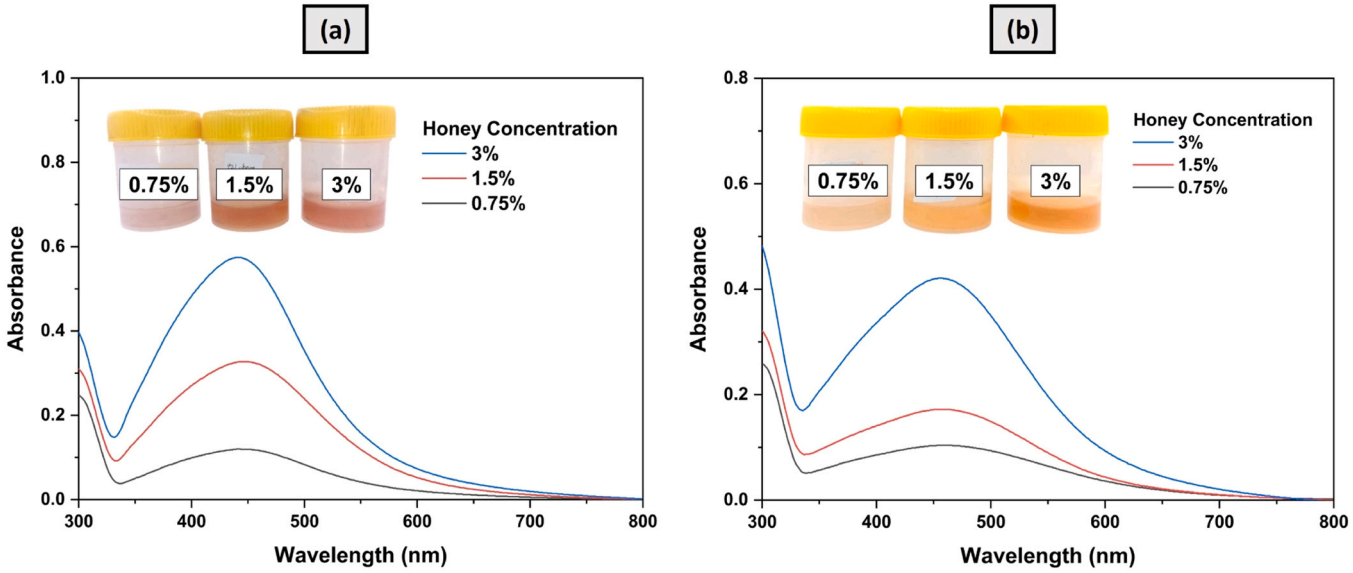

Fig. 4. The effect of Honey Concentration on the synthesis of of AgNPs Cottonwood (a), and AgNPs Rambutan (b).

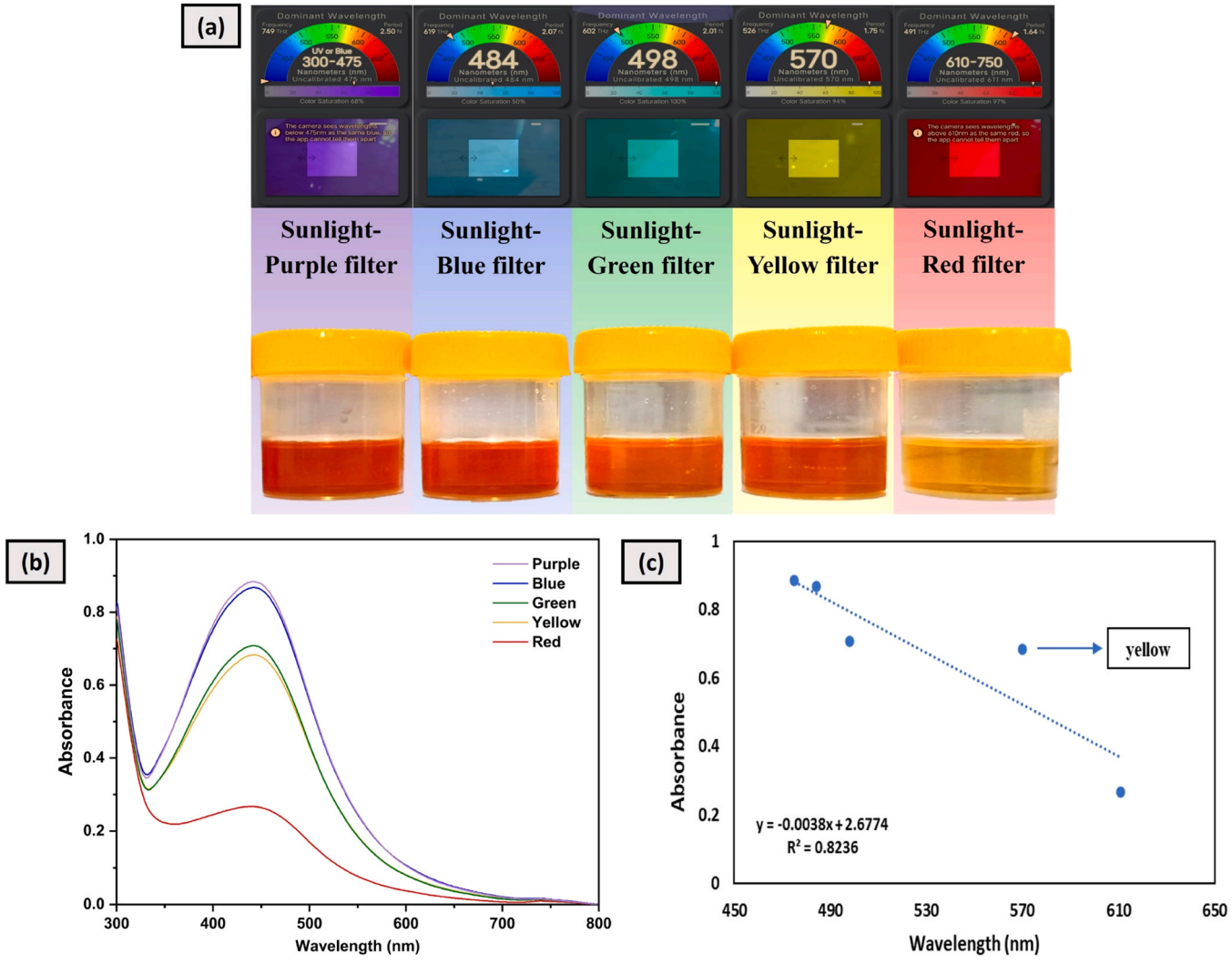

Fig. 5. The effect of wavelength exposure on the synthesis of AgNPs Cottonwood: (a) Measurement of filter wavelengths using a spectrometer alongside images of synthesized AgNP colloids; (b) UV-Vis spectra of AgNPs synthesized under various wavelength exposures; and (c) Linear regression showing the relationship between exposure wavelength and UV-Vis absorbance of synthesized AgNPs.

AgNPs formation, with cottonwood honey demonstrating superior reducing capabilities compared to rambutan honey. These findings underscore the direct correlation between the concentration of natural reducing agents in honey and the synthesis efficiency of AgNPs, as clearly reflected in the UV-Vis spectral profiles.

The optimization of wavelength exposure aimed to determine the most impactful wavelength of sunlight on the reduction of silver ions (Ag^+) to AgNPs using cottonwood honey. The UV-Vis spectra reveal that exposure to yellow light (570 nm) produces a significantly higher absorbance spike compared to other wavelengths (purple, blue, green, and red). This result highlights the unique role of yellow light in optimizing the photoreduction process.

The pronounced effect of yellow light can be attributed to its optimal photon energy, which efficiently drives the photochemical reduction of Ag^+ without degrading the active compounds in honey. Phenolics, flavonoids, and enzymes present in cottonwood honey act as reducing and stabilizing agents. Under yellow light exposure, these bioactive compounds absorb sufficient photon energy to facilitate effective electron transfer from the reducing molecules to Ag^+, promoting the rapid formation of AgNPs. This wavelength likely matches the peak absorption of specific bioactive components, enhancing their reactivity and accelerating nanoparticle synthesis.

Conversely, shorter wavelengths such as purple or blue deliver higher photon energies, which may lead to the photodegradation of honey's bioactive molecules, diminishing their reducing efficiency. Meanwhile, longer wavelengths such as red possess insufficient photon energy to initiate the reduction reaction effectively. Yellow light provides a balance, delivering adequate energy for efficient reduction while preserving the structural integrity and functionality of honey's active compounds.

Additionally, yellow light's position in the central region of the visible spectrum ensures better penetration into the solution, increasing the interaction between light and bioactive molecules. This enhanced interaction likely contributes to the observed higher absorbance, indicating a higher concentration or improved quality of the AgNPs produced under yellow light.

Yellow light demonstrates the most significant impact on the formation of AgNPs due to its optimal photon energy, efficient electron transfer facilitation, and minimal degradation of reducing agents. These findings emphasize the critical role of wavelength selection in sunlight-driven photoreduction processes and nanoparticle synthesis.

The morphological analysis using TEM revealed that Cottonwood AgNPs (Fig. 6) exhibit a variable particle size distribution within the nanometer range. The TEM images depict nearly spherical nanoparticles with minimal aggregation, indicating good stability in the dispersion medium. The scale bar in the TEM image confirms that particle sizes range from 2 to 22 nm, with a predominant distribution between 6 and 12 nm. Size distribution analysis based on the histogram indicates an average particle size of 9.01 nm.

Further statistical analysis of the particle size distribution using a lognormal model yielded an R-square (R^2) value of 0.925. This R^2 value represents the goodness of fit of the lognormal model to the size distribution data obtained from TEM. In this context, an R^2 value close to 1 suggests that the lognormal model accurately describes the particle size distribution of AgNPs. The lognormal distribution is commonly employed in nanoparticle size analysis, as nucleation and growth processes typically follow this pattern, where most particles fall within a specific size range, while a smaller fraction exhibits larger sizes due to secondary growth mechanisms or coalescence. The high R^2 value of 0.925 confirms that the size distribution of AgNPs synthesized using Cottonwood honey follows a lognormal pattern with strong statistical reliability. This finding underscores the effectiveness of the synthesis process in achieving a well-controlled particle size distribution, which is crucial for applications in biomedicine, catalysis, and functional materials.

The selection of bioreducing agents in the synthesis of AgNPs is a pivotal factor dictating their size, morphology, and subsequent biological functionalities. As illustrated in Table 2, different bioreducing

Table 2
Studies on the AgNPs size with different bioreductor.

Bioreductor	Particle Size (nm)	Ref
Cottonwood Honey	9.01	This work
Acalypha indica Linn	2.5–14.5	[16]
Aloe vera	18.5	[49]
Syzygium polyanthum	27.69	[50]
Arthrospira platensis	58.68	[51]
Lactobacillus salivarius	79.47	[52]
Heracleum persicum	4–46	[53]
Ziziphora clinopodioides	17–36	[54]

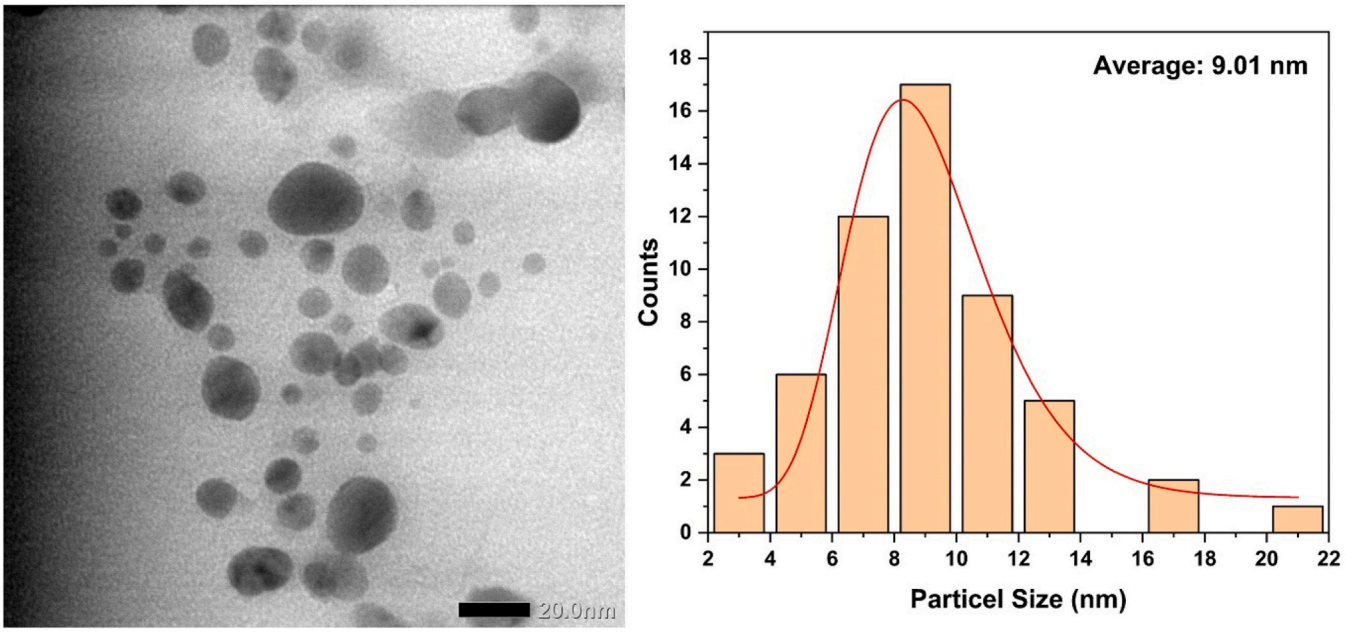

Fig. 6. TEM result (left) and particle distribution calculation (right) of AgNPs Cottonwood.

agents yield AgNPs with markedly distinct size distributions, emphasizing the critical role of biomolecular composition in nanoparticle formation. Cottonwood honey facilitated the synthesis of the smallest AgNPs (9.01 nm), whereas *Lactobacillus salivarius* led to the formation of significantly larger nanoparticles (79.47 nm). This variation can be attributed to the differential presence of polyphenols, flavonoids, proteins, and polysaccharides in each bioreductant, which govern the reduction kinetics of Ag^{+} ions and the stabilization of the resulting nanoparticles [45].

The reduction and stabilization mechanisms of AgNPs are intrinsically linked to the functional groups present within the bioreducing extract. Polyphenolic and flavonoid-rich sources such as *Acalypha indica Linn* (2.5–14.5 nm) and *Aloe vera* (18.5 nm) serve as potent reducing agents, enabling rapid nucleation and yielding smaller, more stable nanoparticles. Conversely, protein- and polysaccharide-rich bioreductants such as *Lactobacillus salivarius* and *Arthrospira platensis* generate larger nanoparticles due to steric hindrance effects, which slow the nucleation phase and favor particle growth.

The size of AgNPs directly dictates their biological reactivity, particularly in antioxidant, antibacterial, and cytotoxic applications. Smaller AgNPs possess a higher surface area-to-volume ratio, enhancing their interaction with biological targets and facilitating Ag^{+} ion release, a key determinant of their bioactivity. AgNPs with a diameter below 20 nm exhibit superior antibacterial properties due to their ability to penetrate bacterial cell membranes efficiently, inducing oxidative stress and membrane disruption [11].

In antioxidant applications, the enhanced surface reactivity of smaller AgNPs allows for more effective scavenging of reactive oxygen species (ROS) and radical stabilization through electron donation [46]. The AgNPs synthesized using *Acalypha indica Linn* and Cottonwood

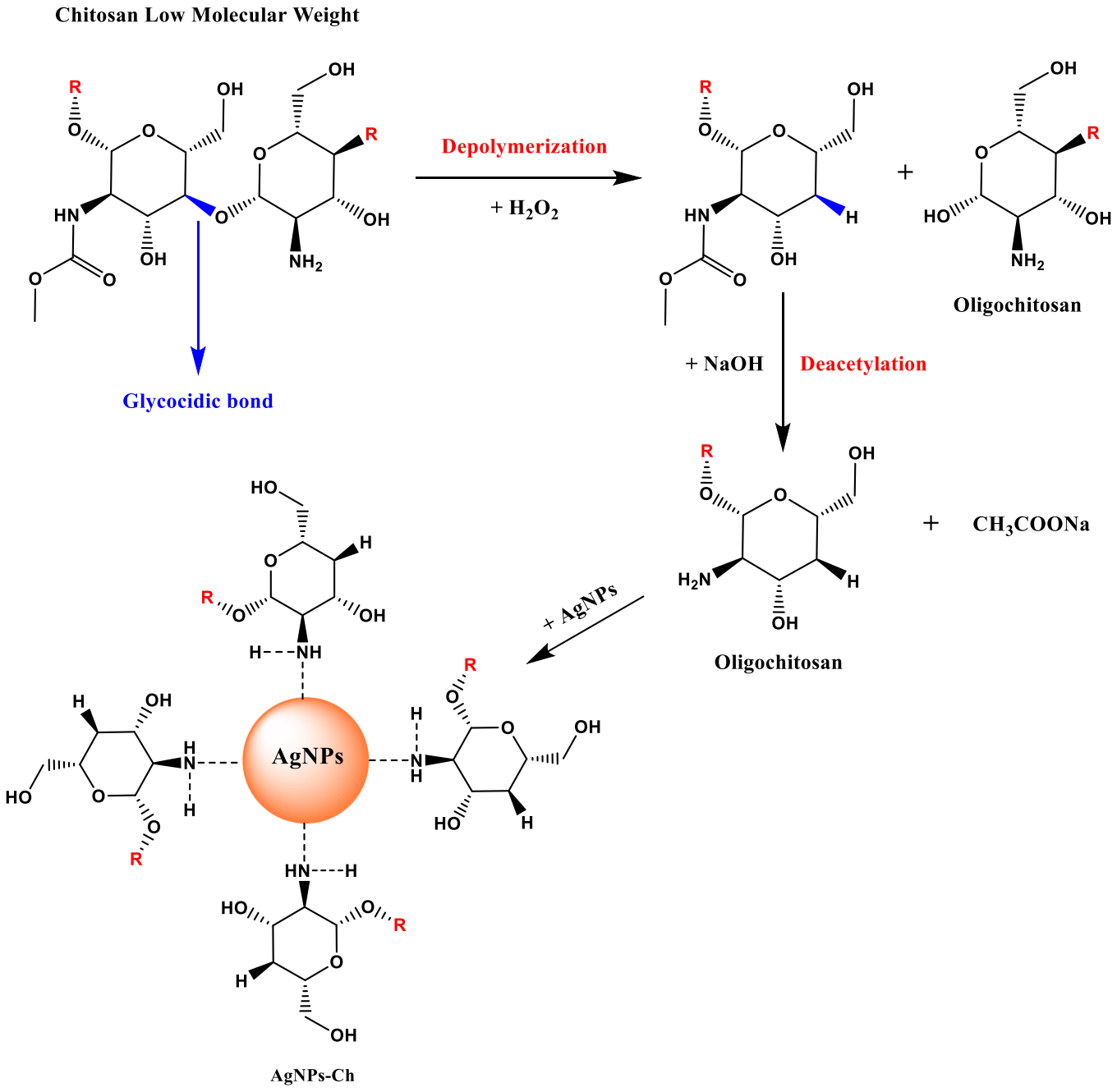

Fig. 7. Conversion of low molecular weight chitosan into oligochitosan via depolymerization and deacetylation reactions, and the interaction of oligochitosan with the AgNPs surface.

honey, which exhibit sub-15 nm dimensions, are expected to demonstrate higher antioxidant potential than their larger counterparts synthesized using *Lactobacillus salivarius* or *Arthrospira platensis*. This effect is further amplified by the retention of biomolecular capping agents on the nanoparticle surface, which provide additional electron-donating capacity.

Furthermore, nanoparticle size critically influences cellular uptake and therapeutic efficacy. Smaller AgNPs undergo endocytosis more efficiently, leading to enhanced intracellular accumulation and potentiated cytotoxicity against cancer cells [47,48]. This size-dependent behavior underscores the necessity of precise control over AgNPs synthesis to optimize their selectivity and therapeutic performance in biomedical applications.

Collectively, these findings highlight the profound influence of bioreducing agents not only on the physicochemical characteristics of AgNPs but also on their functional performance in biomedical applications. A deeper understanding of the structure-function relationship between bioreducing agent composition, particle size, and biological activity will be instrumental in advancing the development of AgNPs for pharmaceutical and nanomedicine applications.

3.3. Coating AgNPs with oligochitosan

In this study, the synthesized AgNPs were coated with modified chitosan. This modification involved transforming low molecular weight chitosan into water-soluble chitosan, known as oligochitosan. The mechanism illustrates (Fig. 7) the depolymerization of low molecular weight chitosan into oligochitosan through a reaction with hydrogen peroxide (H_2O_2), followed by deacetylation using sodium hydroxide (NaOH). The depolymerization step involves the cleavage of glycosidic bonds within the chitosan structure, facilitated by the oxidative action of H_2O_2, resulting in shorter oligosaccharide chains known as oligochitosan. Subsequently, the deacetylation process removes acetyl groups from the chitosan backbone, increasing the number of free amino groups, which enhances solubility in water and reactivity. The final product, oligochitosan, is a water-soluble, simplified form of chitosan that is particularly suited for advanced applications such as coating AgNPs.

Coating AgNPs with chitosan, especially oligochitosan, provides several advantages in terms of stability, biological efficacy, and biocompatibility. Firstly, the chitosan coating enhances the colloidal stability of AgNPs by preventing aggregation through steric and electrostatic stabilization mechanisms. The free amino groups in chitosan can form coordination bonds with the silver nanoparticle surface, creating a robust protective layer that maintains nanoparticle dispersion and prevents clustering. Secondly, chitosan contributes to improved biological functionality of AgNPs. Known for its inherent antimicrobial and antioxidant properties, chitosan synergistically amplifies the bioactivity of AgNPs. The amino and hydroxyl groups in chitosan act as scavengers for reactive oxygen species, enhancing the antioxidant capabilities of the coated nanoparticles, which are valuable for applications in pharmaceuticals and healthcare.

Moreover, the chitosan coating significantly reduces the totoxicity commonly associated with uncoated AgNPs. Free silver ions (Ag^+) released from uncoated nanoparticles are a major source of toxicity in biological systems. The chitosan layer serves as a diffusion barrier, controlling the release of silver ions and mitigating adverse effects on healthy cells. This improved biocompatibility broadens the potential of chitosan-coated AgNPs for safe and effective use in medical and biotechnological applications.

The UV-Vis spectra (Fig. 8) presented indicate distinct absorption peaks for each sample, reflecting the unique characteristics of AgNPs influenced by chitosan coating and the type of honey used as a reducing agent. These absorption peaks are typically associated with localized surface plasmon resonance (LSPR), a hallmark of metallic nanoparticles such as AgNPs.

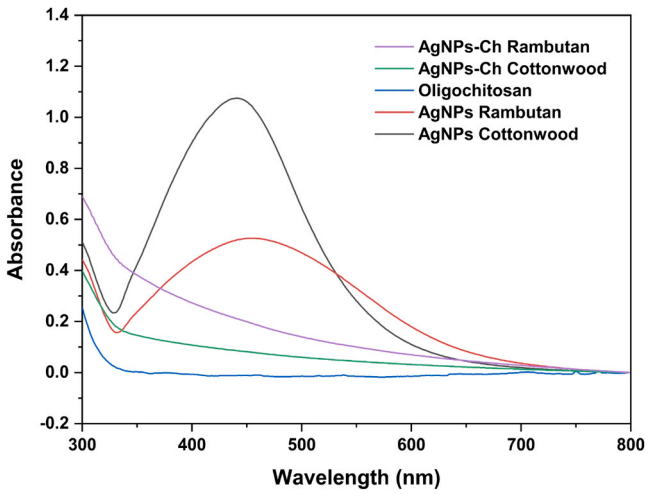

Fig. 8. The UV–vis spectra of AgNPs, Oligochitosan and oligochitosan-coated AgNPs.

The spectrum of oligochitosan-coated AgNPs with Cottonwood honey bioreductor (AgNPs-Ch Cottonwood) closely resembles that of oligochitosan, characterized by the absence of the distinctive LSPR peak at 420 nm. This absence indicates that the AgNPs have been effectively encapsulated within the oligochitosan matrix, with the observed absorption predominantly reflecting oligochitosan properties. This suggests that chitosan coating on AgNPs reduced with cottonwood honey facilitates a stronger interaction between the nanoparticle surface and the chitosan layer. Consequently, the encapsulation process is more efficient, resulting in a stable electron distribution at the nanoparticle surface that aligns with the intrinsic characteristics of oligochitosan.

In contrast, the spectrum of oligochitosan-coated AgNPs with Rambutan honey bioreductor (AgNPs-Ch Rambutan) displays a broader absorption peak with lower intensity, diverging significantly from the oligochitosan spectrum. This indicates less optimal chitosan coating for AgNPs reduced using rambutan honey, likely due to differences in the chemical composition of the two types of honey. The higher phenolic, flavonoid, and reducing sugar content in cottonwood honey may enhance the reduction process and improve compatibility with chitosan, enabling more uniform coating.

These findings underscore the critical role of the reducing agent in tailoring nanoparticle properties and achieving efficient chitosan encapsulation. AgNPs-Ch Cottonwood, with its well-defined oligochitosan-like spectrum, demonstrates superior coating uniformity and stability, highlighting its potential for applications requiring consistent and well-encapsulated nanomaterials.

The FTIR spectra (Fig. 9) provide a comprehensive understanding of the molecular interactions occurring during the synthesis of AgNPs using honey as a bioreductor and the subsequent capping process with oligochitosan. The broad absorption peaks observed in the 3000–3500 cm^{-1} region, corresponding to O-H stretching vibrations, are indicative of hydroxyl groups present in the honey, AgNPs, and AgNPs-Chitosan samples. These functional groups originate from phenolic compounds, flavonoids, proteins, and sugars such as glucose and fructose, which serve as primary reducing agents in the synthesis of AgNPs. Additionally, N-H stretching vibrations from the amino groups in oligochitosan are evident, confirming their critical role in stabilizing the nanoparticles. This region demonstrates the importance of both the reducing and capping agents in the synthesis process.

Low-intensity bands around 2930 cm^{-1}, associated with C-H stretching vibrations, are present in the honey, AgNPs, and AgNPs-Chitosan samples, further confirming the involvement of organic compounds from honey in nanoparticle stabilization. Notably, significant changes in the 1640–1730 cm^{-1} range, corresponding to C═O stretching

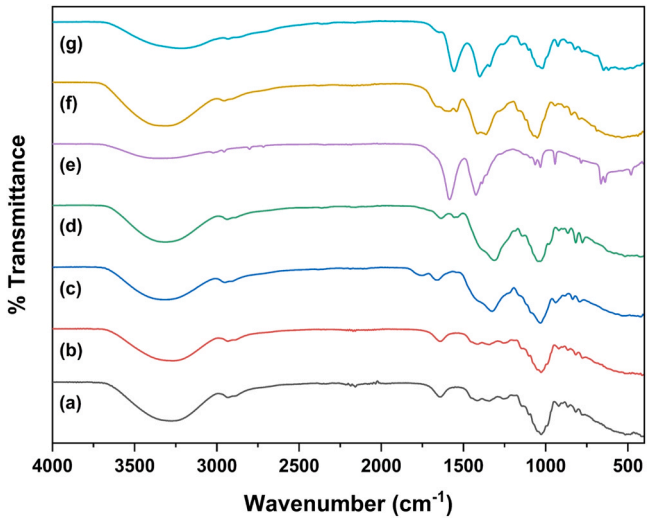

Fig. 9. The FTIR spectra of Cottonwood honey (a); Rambutan honey (b); AgNPs Cottonwood (c); AgNPs Rambutan (d); Oligochitosan (e); AgNPs-Ch Cottonwood (f); and AgNPs-Ch Rambutan (g).

vibrations of aldehydes and ketones in glucose and fructose, highlight the chemical modifications during AgNPs formation. In honey samples, these groups exhibit strong absorption peaks, which shift and decrease in intensity in the AgNPs spectra, indicating electron donation from carbonyl groups as a key mechanism in AgNPs reduction. For AgNPs Cottonwood, the emergence of overlapping peaks around 1639 cm^{-1} and 1730 cm^{-1} suggests strong interactions between carbonyl groups and the AgNPs surface.

The amine groups of oligochitosan play a pivotal role in the capping process, as evidenced by significant intensity reductions in the 1560–1570 cm^{-1} range for the AgNPs-Chitosan samples compared to oligochitosan alone. This interaction is particularly pronounced for AgNPs-Ch Cottonwood, indicating a robust interaction between the amino groups of oligochitosan and the nanoparticle surface. This finding underscores the enhanced compatibility of cottonwood honey as a reducing agent in facilitating stable capping. Furthermore, absorption bands in the 1390–1405 cm^{-1} range, attributed to C-O-C stretching vibrations in cyclic structures, are evident in both oligochitosan and AgNPs-Chitosan samples, confirming the integration of chitosan in the nanoparticle structure.

Unique peaks in the 1300–1310 cm^{-1} region, observed only in the AgNPs spectra, correspond to C-O or C-H vibrations, indicating the presence of organic stabilizers from honey on the nanoparticle surface. These organic components play a crucial role in preventing nanoparticle aggregation and enhancing stability. Additionally, the region between 1000 and 1050 cm^{-1} reveals peaks associated with hydroxyl (-OH) and C-O stretching vibrations, likely derived from sugars or polysaccharides in honey, further contributing to nanoparticle formation and stability.

Comparative analysis highlights the superior performance of cottonwood honey in both nanoparticle synthesis and capping. AgNPs synthesized with cottonwood honey exhibit stronger interactions, as reflected by more pronounced shifts and intensity changes in key FTIR regions. This can be attributed to the higher phenolic and flavonoid content in cottonwood honey, which enhances the reduction process and promotes better compatibility with oligochitosan. In contrast, AgNPs synthesized with rambutan honey display weaker interactions, with less significant changes in FTIR peak intensities and shifts, suggesting a less efficient reduction process and weaker capping interactions.

The physicochemical properties (Table 3) of the synthesized AgNPs and chitosan-coated AgNPs (AgNPs-Ch) provide crucial insights into their colloidal stability, size distribution, and potential biomedical applications. The zeta potential, polydispersity index (PI), and hydrodynamic size (Z-average) serve as fundamental indicators of dispersion stability and aggregation tendencies.

Table 3
Zeta potential and colloidal stability of AgNPs and AgNPs-Ch.

Parameter	Cottonwood Honey Bioreductor		Rambutan Honey Bioreductor	
	AgNPs	AgNPs-Ch	AgNPs	AgNPs-Ch
Z-Average (nm)	44.16	454.81	45.00	461.32
Polydispersity Index (PI)	0.36	0.37	0.33	0.33
Zeta Potential (mV)	−0.99	5.24	−0.11	5.49
Conductivity (mS/cm)	1.01	1.33	0.71	1.33
Wall Zeta Potential (mV)	−3.61	−0.44	−0.52	−0.48
Quality Factor	1.02	1.69	0.38	1.09

Zeta potential plays a critical role in determining the stability of colloidal nanoparticles by reflecting the magnitude of electrostatic repulsion between particles. In general, nanoparticles with zeta potential exceeding ± 30 mV exhibit strong repulsive forces that prevent aggregation, while values close to zero indicate a propensity for particle agglomeration.

For the uncoated AgNPs, the zeta potential was measured at −0.99 mV (AgNPs Cottonwood) and −0.11 mV (AgNPs Rambutan), suggesting weak electrostatic stabilization. The negative surface charge can be attributed to the presence of biomolecules from honey acting as capping agents, though their charge density appears insufficient to impart robust stability. Upon modification with chitosan, the zeta potential significantly shifted to + 5.24 mV (AgNPs-Ch Cottonwood) and + 5.49 mV (AgNPs-Ch Rambutan). This positive shift is expected, given that chitosan contains protonated amine groups at acidic pH, which enhance the surface charge of nanoparticles. However, the observed values remain well below the ± 30 mV threshold for electrostatic stability, indicating that steric hindrance rather than electrostatic repulsion may be the primary stabilization mechanism in AgNPs-Ch.

The wall zeta potential values, which describe the electrical potential at the nanoparticle-liquid interface, further reinforce this observation. The negative values for AgNPs (-3.61 mV for AgNPs Cottonwood and −0.52 mV for AgNPs Rambutan) suggest weak surface charge stabilization. After chitosan coating (AgNPs-Ch), these values shift closer to zero (-0.44 mV and −0.48 mV), implying reduced electrostatic stabilization, which aligns with the increase in hydrodynamic size.

The Z-average values, representing the intensity-weighted hydrodynamic diameter, provide critical insights into nanoparticle size and dispersion. The uncoated AgNPs exhibit small, well-dispersed sizes of 44.16 nm (AgNPs Cottonwood) and 45.00 nm (AgNPs Rambutan), indicating precise control over nucleation and growth during biosynthesis.

Upon modification with oligochitosan, the hydrodynamic diameter increases significantly to 454.81 nm (AgNPs Cottonwood) and 461.32 nm (AgNPs Rambutan). This substantial increase does not indicate nanoparticle aggregation but rather results from the oligochitosan layer enveloping the AgNPs. Oligochitosan, as a hydrophilic polymer, forms a hydrated shell around the nanoparticles, contributing to the larger hydrodynamic size measured by Dynamic Light Scattering (DLS). This phenomenon is commonly observed in polymer-coated nanoparticles, where the hydration layer significantly influences the detected particle size.

It is crucial to emphasize that while the hydrodynamic size increases, colloidal stability is primarily dictated by the zeta potential rather than particle diameter alone. The shift toward a more positive zeta potential following oligochitosan modification indicates enhanced electrostatic interactions due to the protonated amine groups on the polymer. Therefore, the observed increase in Z-average is not a consequence of aggregation but rather an expected outcome of successful oligochitosan coating on AgNPs.

The polydispersity index (PI) is a crucial parameter in nanoparticle

characterization, representing the size distribution uniformity. Typically, PI values below 0.3 indicate monodisperse systems, while values above 0.3 suggest moderate to high heterogeneity in particle size distribution. The PI values of AgNPs Cottonwood and AgNPs Rambutan were 0.36 and 0.33, respectively, indicating a moderately broad size distribution. After chitosan modification, PI values remained relatively unchanged (0.37 for AgNPs-Ch Cottonwood and 0.33 for AgNPs-Ch Rambutan), signifying that while the mean particle size increased significantly, the overall distribution range did not broaden drastically.

Conductivity measurements provide additional insights into the ionic environment of the nanoparticle dispersions. The uncoated AgNPs exhibit moderate conductivity (1.01 mS/cm for AgNPs Cottonwood and 0.71 mS/cm for AgNPs Rambutan), which may arise from the presence of ionic species in the honey matrix. Interestingly, the conductivity increases after chitosan modification (1.33 mS/cm for both samples), suggesting enhanced ionic interactions, possibly due to the presence of protonated amine groups from chitosan, which contribute to the overall ionic strength of the dispersion.

The quality factor, which combines multiple stability indicators, further supports the observed aggregation trends. The initial AgNPs exhibited relatively stable values (1.02 for AgNPs Cottonwood and 0.38 for AgNPs Rambutan), whereas after chitosan coating, the quality factor increased to 1.69 for AgNPs-Ch Cottonwood but also increased for AgNPs-Ch rambutan (1.09). The higher quality factor in AgNPs-Ch suggests a shift in stability mechanisms, where steric stabilization dominates over electrostatic forces.

Optimization analysis based on UV-Vis, FTIR and PSA-DLS revealed that AgNPs synthesized using Cottonwood honey exhibited superior characteristics and enhanced stability, particularly during the coating process with oligochitosan. Consequently, further characterization using XRD and FESEM-EDX was exclusively conducted on AgNPs Cottonwood and AgNPs-Ch Cottonwood samples to gain deeper insights into the structural and morphological properties of AgNPs following oligochitosan coating.

The crystalline structure of AgNPs was investigated using XRD, as illustrated in the diffractogram (Fig. 10). The XRD pattern of AgNPs synthesized using cottonwood honey exhibits distinct peaks at 2θ angles of 37.79°, 44.03°, 64.28°, 77.08°, and 81.47°. These peaks align well with the standard reference for silver nanoparticles (JCPDS card No. 04–0783), corresponding to the (111), (200), (220), (311), and (222) planes of the face-centered cubic (FCC) structure of metallic silver. The intense peak at 37.84°, attributed to the (111) plane, represents the preferred orientation of the AgNP crystals, further confirming the formation of crystalline AgNPs. This pattern highlights the effectiveness of cottonwood honey as a bioreductant in facilitating the synthesis of high-purity AgNPs.

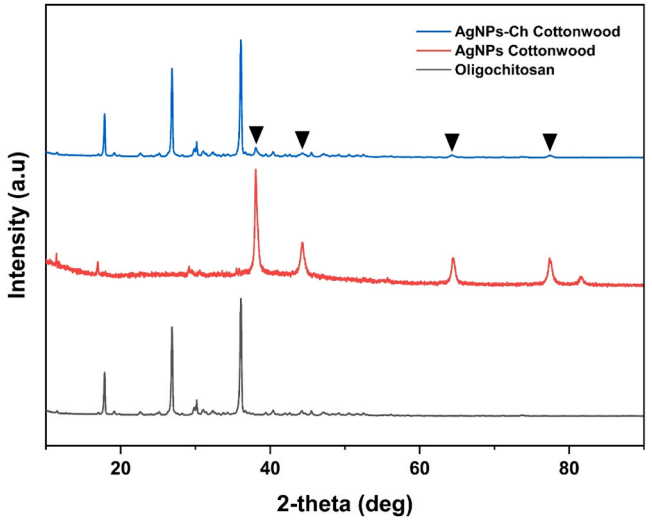

Fig. 10. The XRD pattern of AgNPs-Cottonwood, Oligochitosan, and AgNPs-Ch Cottonwood.

The crystallite size of the AgNPs was estimated using the Debye-Scherrer equation, focusing on the most intense peak at 2θ = 37.79°. This peak was selected for its sharpness and high intensity, which minimizes the influence of background noise and other secondary phases. With a full width at half maximum (FWHM) of 0.1673°, the average crystallite size of the AgNPs was calculated to be approximately 51.20 nm. This nanoscale size underscores the potential of the green synthesis approach using cottonwood honey in producing well-defined nanoparticles with controlled size and morphology.

The XRD pattern of oligochitosan exhibits its most intense peak at 2θ = 36.11°, followed by additional prominent peaks at 26.88°, 17.87°, and 30.15°. These diffraction peaks indicate the semicrystalline nature of oligochitosan, with a significant contribution from crystalline regions, particularly at 2θ = 36.11°. This pattern reflects a degree of structural order within the polymer chains of oligochitosan, suggesting the presence of well-defined crystalline domains interspersed with amorphous regions.

Interestingly, the XRD pattern of the AgNPs-Ch Cottonwood composite demonstrates significant overlap with the pattern of pure oligochitosan, indicating that the AgNPs are well incorporated into the oligochitosan matrix. While the characteristic peaks of AgNPs (e.g., at 2θ = 37.79°, 44.03°, 64.28°, and 77.08°) are still present, their intensities are significantly diminished compared to those observed for standalone AgNPs. This suggests that the AgNPs are effectively embedded within the oligochitosan matrix, leading to a reduction in peak sharpness and intensity due to the interaction between the nanoparticle surface and the oligochitosan chains.

The diminished intensity of the AgNPs peaks in the composite highlights the robust encapsulation of the nanoparticles by the oligochitosan matrix, which may contribute to enhanced stability and reduced aggregation of the AgNPs. This interaction is further supported by the semi-crystalline nature of the composite, which is dominated by the oligochitosan matrix but retains the structural characteristics of AgNPs. Such a configuration is desirable for applications requiring stabilized nanoparticles with functional biopolymer coatings, such as in biomedical and antimicrobial fields. The results underscore the synergistic effect of cottonwood honey and oligochitosan in producing nanocomposites with favorable physicochemical properties.

The Field Emission Scanning Electron Microscopy-Energy Dispersive X-ray Spectroscopy (FESEM-EDX) analysis of oligochitosan (Fig. 11) reveals a highly heterogeneous surface morphology characterized by an irregular, porous structure, as observed in the FESEM image. This porous architecture underscores the material's suitability for applications such as drug delivery or adsorption, where increased surface area plays a pivotal role in enhancing functionality.

The EDX spectrum identifies key elemental components, namely carbon (C), oxygen (O), nitrogen (N), and sodium (Na), with atomic percentages of 76.40 %, 22.74 %, 0.75 %, and 0.11 %, respectively. The dominance of carbon is consistent with the polysaccharide backbone of oligochitosan, predominantly composed of glucosamine units. The substantial presence of oxygen is attributed to hydroxyl and carbonyl functional groups inherent to the oligosaccharide structure. Meanwhile, the nitrogen content, though relatively low, originates from the amino groups characteristic of chitosan. The trace sodium likely stems from residual reagents or buffer components used during sample preparation.

In the EDX spectrum, the characteristic energy peaks are observed at approximately 0.277 keV (C), 0.525 keV (O), 0.392 keV (N), and 1.041 keV (Na), with corresponding counts per second per electron volt (cps/eV) reflecting the relative abundance of each element. The pronounced intensity of the carbon peak aligns with the material's carbon-rich composition.

Elemental mapping further corroborates these findings, displaying a uniform distribution of carbon (red) and oxygen (green) across the

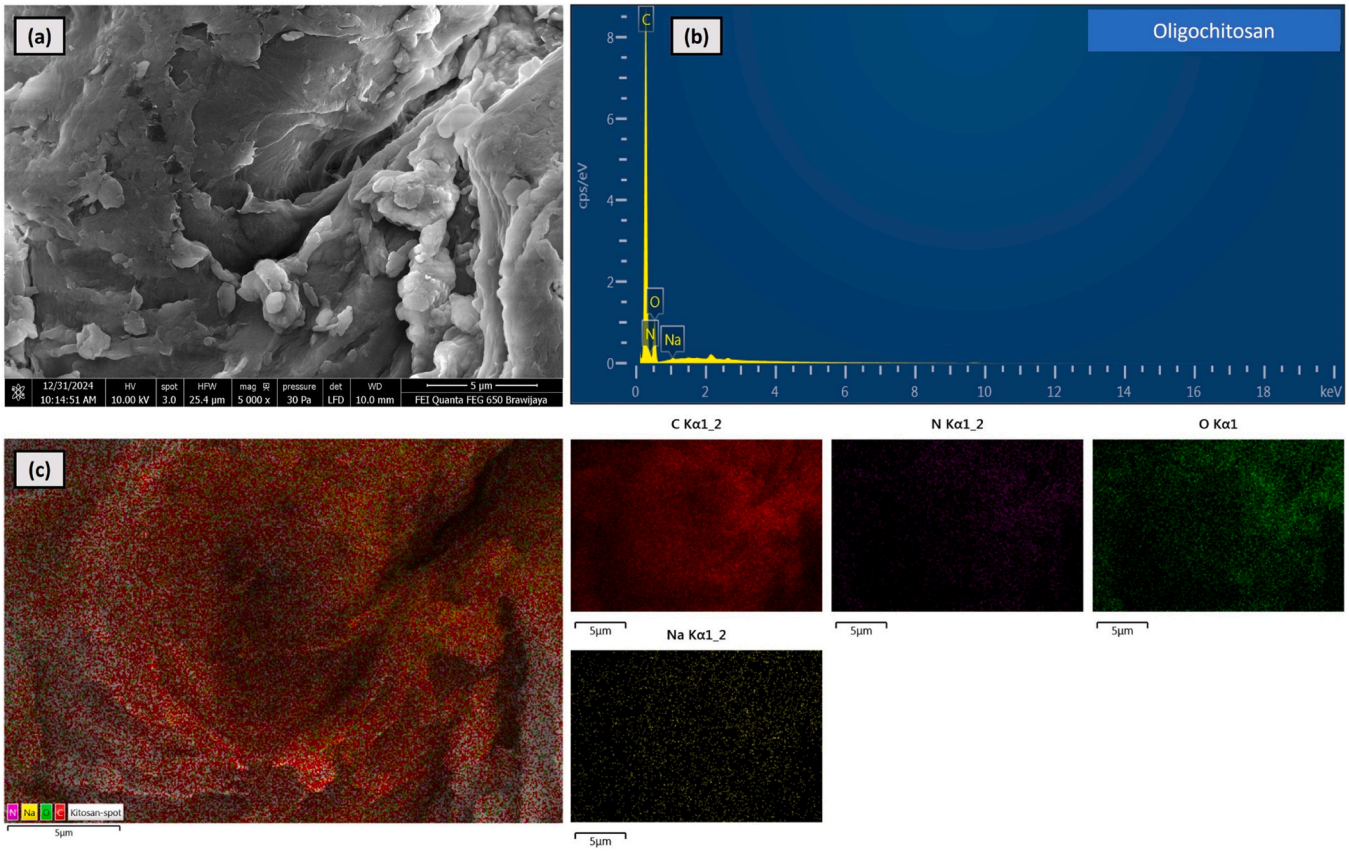

Fig. 11. FESEM-EDX results of Oligochitosan: (a) SEM image at 5000 × magnification; (b) EDX spectra; and (c) EDX elemental mapping.

analyzed region. Nitrogen (purple) and sodium (yellow), while present in minor quantities, are also evenly dispersed, indicating homogeneity in the chemical composition of oligochitosan. The overlay map provides a comprehensive visualization, affirming the uniformity of elemental distribution and chemical integrity throughout the material.

These results establish oligochitosan as a carbon-rich polymer with significant oxygen content and traces of nitrogen, reflecting its fundamental biopolymer structure. The observed morphology and elemental composition are highly advantageous for biomedical and environmental applications, such as bioactive molecule delivery or pollutant adsorption, where material stability, biocompatibility, and surface characteristics are critical determinants of performance.

The FESEM-EDX analysis of AgNPs synthesized using cottonwood honey (AgNPs Cottonwood) as a reducing and stabilizing agent reveals a well-defined nanostructure with a uniform particle size distribution. The FESEM micrograph illustrates (Fig. 12) nanoparticles ranging from 5 to 35 nm in size, with an average diameter of 11.71 nm, as determined by ImageJ software. The narrow size distribution and small particle size demonstrate the effectiveness of cottonwood honey in producing stable and homogeneously dispersed AgNPs, critical for applications in catalysis, antimicrobial activity, and other nanotechnological advancements.

The EDX spectrum confirms the presence of key elements, namely carbon (C), oxygen (O), nitrogen (N), and silver (Ag), with atomic percentages of 38.04 %, 15.81 %, 21.98 %, and 24.17 %, respectively. The high carbon content reflects the organic composition of cottonwood honey, rich in reducing agents such as polyphenols and sugars. Oxygen likely originates from hydroxyl and carbonyl groups within these organic compounds, playing a crucial role in reducing Ag^{+} ions to Ag^{0}. Nitrogen may be attributed to amino groups or protein-based components in the honey, which act as stabilizing agents, further preventing nanoparticle aggregation. The substantial silver content (24.17 %) confirms the successful reduction of Ag^{+} ions and the subsequent formation of AgNPs.

Characteristic energy peaks in the EDX spectrum appear at 0.277 keV (C), 0.525 keV (O), 0.392 keV (N), and 2.984 keV (Ag), with the silver peak exhibiting the highest cps/eV intensity. This high intensity corresponds to the abundance of metallic silver within the sample. The strong carbon and oxygen signals further support the presence of an organic coating derived from cottonwood honey, which encapsulates the AgNPs and contributes to their stability.

Elemental mapping demonstrates a homogeneous distribution of silver (blue), carbon (red), oxygen (green), and nitrogen (purple) across the analyzed area. The composite elemental map highlights the uniform dispersion of AgNPs without significant aggregation, underscoring the stabilizing effect of the organic components from cottonwood honey. This even distribution is essential for ensuring consistent material properties and enhanced functionality.

The use of cottonwood honey as a reducing and stabilizing agent offers several advantages, including sustainability, environmental friendliness, and the ability to produce nanoparticles with precise size control. The presence of bioactive compounds such as polyphenols in the honey not only facilitates the reduction process but also imparts additional functional properties to the AgNPs.

The FESEM-EDX analysis of AgNPs synthesized using cottonwood honey as a bioreductant and coated with oligochitosan (AgNPs-Ch Cottonwood) reveals significant structural and elemental characteristics (Fig. 13). The FESEM micrograph indicates that the nanoparticles exhibit a size range of 30–150 nm, with an average diameter of 87.81 nm as calculated via ImageJ software. The relatively larger particle size compared to uncoated AgNPs (11.71 nm) observed in previous studies suggests the presence of a thick oligochitosan coating, which stabilizes and encapsulates the nanoparticles.

The EDX spectrum confirms the elemental composition, with atomic percentages of 38.78 % for carbon (C), 32.11 % for oxygen (O), 14.30 %

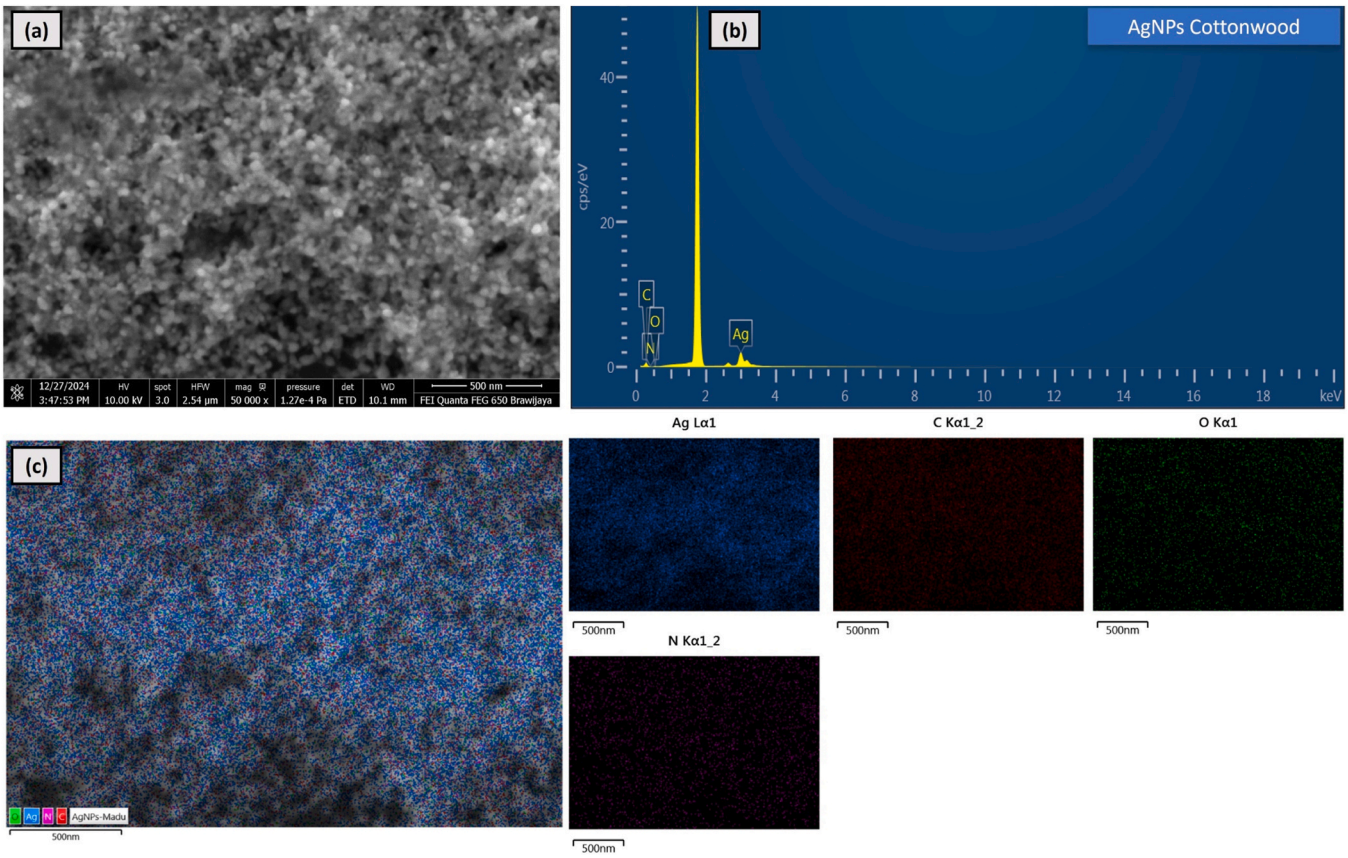

Fig. 12. FESEM-EDX result of AgNPs Cottonwood: (a) SEM image at 50,000 × magnification; (b) EDX spectra; and (c) EDX elemental mapping.

for nitrogen (N), 6.94 % for silver (Ag), 5.13 % for sodium (Na), and 2.75 % for phosphorus (P). The high carbon and oxygen content underscores the dominant contribution of oligochitosan as a stabilizing matrix. Oligochitosan, a biopolymer derived from chitosan, is known for its abundant hydroxyl (-OH) and amino (-NH_2) functional groups, which likely account for the significant oxygen and nitrogen signals. The silver content, although lower than in uncoated AgNPs, remains indicative of successful nanoparticle synthesis and suggests effective encapsulation within the biopolymer matrix.

The characteristic energy peaks for each element are observed at 0.277 keV (C), 0.525 keV (O), 0.392 keV (N), 1.041 keV (Na), 2.013 keV (P), and 2.984 keV (Ag). Among these, the silver peak exhibits a moderate cps/eV intensity, reflecting its lower relative abundance compared to organic components but still confirming its core presence within the composite. The strong signals for carbon, oxygen, and nitrogen correspond to the oligochitosan coating, while the presence of sodium and phosphorus can be attributed to residual components from the cottonwood honey bioreduction process or chitosan modification.

Elemental mapping illustrates a homogeneous distribution of Ag (blue), C (red), O (green), N (purple), Na (yellow), and P (orange) across the observed region. The uniform dispersion of silver corroborates the effectiveness of oligochitosan in preventing nanoparticle aggregation, while the co-localization of nitrogen and oxygen indicates the presence of functional groups from the biopolymer matrix. This uniform distribution highlights the synergistic interaction between AgNPs and oligochitosan, ensuring material stability and functionality.

The observed particle size increase and compositional changes are consistent with the expected effects of oligochitosan coating, which introduces a thick organic layer around the AgNPs. The bioreduction process using cottonwood honey, rich in polyphenols and reducing sugars, contributes to the initial formation of nanoparticles, while oligochitosan enhances stability through electrostatic and hydrogen bonding interactions. Additionally, the presence of phosphorus and sodium, derived from honey components or oligochitosan modification, further supports the stability and functionalization of the composite.

These findings demonstrate the potential of AgNPs-Ch Cottonwood as a biocompatible and multifunctional nanomaterial. The controlled particle size, uniform distribution, and presence of bioactive functional groups make it suitable for advanced applications in biomedicine, antimicrobial systems, and environmental remediation. The synergistic effect of cottonwood honey as a bioreductant and oligochitosan as a stabilizer ensures both material performance and sustainability.

3.4. *In vitro antioxidant activity test*

The antioxidant activity of Cottonwood honey was slightly higher than that of Rambutan honey (Fig. 14), as indicated by their respective IC_{50} values (1519.53 μg/mL for Cottonwood honey vs. 1662.09 μg/mL for Rambutan honey). This subtle difference can be attributed to variations in the chemical composition of the two types of honey. Cottonwood honey is likely to contain higher levels of phenolic compounds and flavonoids, which are well-known for their ability to neutralize free radicals by donating electrons or hydrogen atoms. These bioactive compounds contribute significantly to the overall antioxidant capacity of honey.

The profile of reducing sugars, such as glucose and fructose, also plays a role in the antioxidant activity of honey. These sugars can interact with reactive oxygen species (ROS) and reduce their reactivity, albeit less effectively than phenolic compounds. The superior antioxidant performance of Cottonwood honey might also be influenced by its botanical origin, which provides a broader diversity of bioactive compounds compared to Rambutan honey. Furthermore, variations in physicochemical properties such as pH and water activity (Aw) could

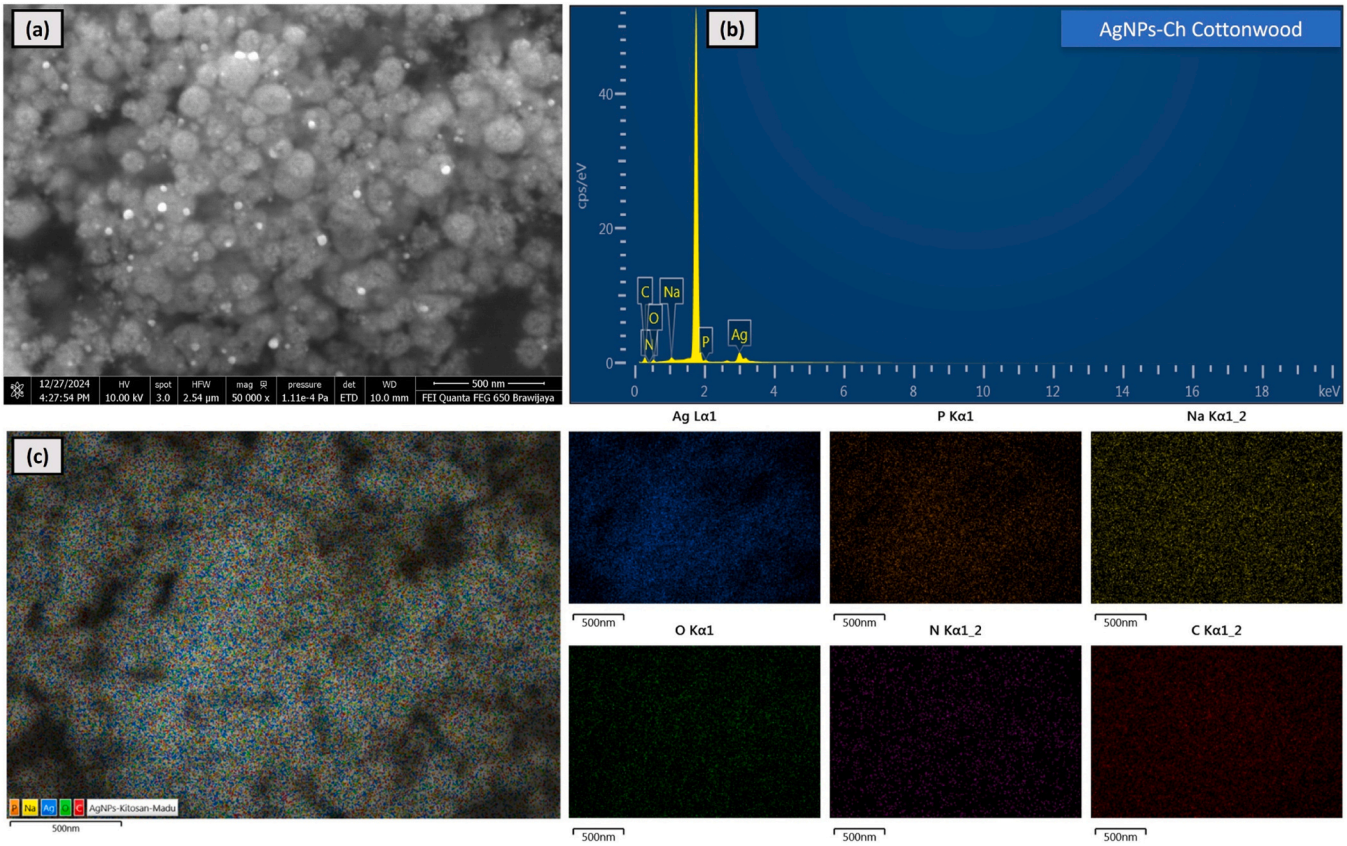

Fig. 13. FESEM-EDX result of AgNPs-Ch Cottonwood: (a) SEM image at 50,000 × magnification; (b) EDX spectra; and (c) EDX elemental mapping.

affect antioxidant activity. Cottonwood honey, if possessing a slightly lower pH, might stabilize its bioactive compounds more effectively, contributing to its enhanced antioxidant performance.

In conclusion, while the antioxidant activity of Cottonwood honey is only marginally higher than that of Rambutan honey, this difference reflects the influence of its phenolic and flavonoid content, mineral composition, sugar profile, and physicochemical properties. These findings underscore the significance of the botanical origin of honey in determining its antioxidant capacity and potential applications in health-related formulations.

The coating of AgNPs with oligochitosan significantly enhanced their antioxidant activity, as indicated by a dramatic reduction in IC_{50} values (Table 4) for AgNPs-Ch Cottonwood (430.95 ± 1.53 μg/mL) and AgNPs-Ch Rambutan (551.29 ± 5.09 μg/mL) compared to uncoated AgNPs (AgNPs Cottonwood: 1468.75 ± 2.74 μg/mL; AgNPs Rambutan: 1519.53 ± 3.41 μg/mL). These results highlight a substantial increase in antioxidant activity after oligochitosan coating, with improvements of 3.41-fold and 3.01-fold for AgNPs synthesized using cottonwood and rambutan honey, respectively. This remarkable enhancement can be attributed to multiple mechanisms, including the role of oligochitosan as a stabilizing coating agent, an effective nanocarrier, and a key component in the nanoencapsulation process.

The antioxidant activity of the tested samples, as indicated by their IC_{50} values, revealed statistically significant differences (ANOVA, $F = 44{,}450.18$, $p < 0.0001$). Post-hoc Tukey HSD analysis further delineated these differences, classifying the samples into distinct statistical groups ($p < 0.05$, Table 4). Honey samples (Cottonwood and Rambutan) exhibited the highest IC_{50} values (1519.53–1662.09 μg/mL, group *b-c*), suggesting relatively lower antioxidant activity. A comparable trend was observed for AgNPs synthesized using honey (AgNPs Cottonwood: 1468.75 μg/mL, AgNPs Rambutan: 1519.53 μg/mL), where the reduction in IC_{50} was statistically insignificant compared to honey alone, indicating that AgNPs formation did not markedly enhance antioxidant potential ($p > 0.05$).

In contrast, Oligochitosan demonstrated a substantial decrease in IC_{50} (665.98 μg/mL, group *d*), reflecting significantly enhanced antioxidant capacity. Notably, the incorporation of chitosan in AgNPs (AgNPs-Ch) resulted in the most pronounced antioxidant activity (IC_{50} = 430.95–551.29 μg/mL, group *e*), significantly distinct from all other groups ($p < 0.0001$). This suggests a synergistic effect between chitosan and AgNPs, likely attributed to chitosan's ability to stabilize nanoparticles and enhance radical scavenging activity. The statistical stratification underscores the role of chitosan modification in augmenting the antioxidant efficacy of AgNPs, positioning AgNPs-Ch as a superior candidate for biomedical and pharmaceutical applications requiring potent antioxidant properties.

Despite the antioxidant IC_{50} values of AgNPs Cottonwood (1468.75 ± 2.74 μg/mL) and AgNPs Rambutan (1519.53 ± 3.41 μg/mL) not exhibiting superior performance compared to certain AgNPs synthesized using alternative bioreducing agents—such as *Caesalpinia pulcherrima* (664 μg/mL) [55], *Clinacanthus nutans* (434.60 μg/mL) [56], and *Zea mays L.* (385.87 μg/mL) [57]—this study presents a strategic approach to address the inherent limitations of AgNPs in antioxidant applications. A critical challenge in nanobiotechnology lies in optimizing the bioactivity of AgNPs, particularly when their inherent antioxidant capacity is suboptimal. In this context, polymeric surface modifications, such as chitosan coating, emerge as a viable strategy to enhance their functional efficacy. In this study, following the surface modification with oligochitosan, the resulting IC_{50} values were found to be comparable to or slightly improved over those reported in previous studies [55–57]. The oligochitosan coating not only enhanced the biological activity of the material but also contributed to improved biocompatibility, underscoring its potential for safe application in daily-use biomedical and environmental settings.

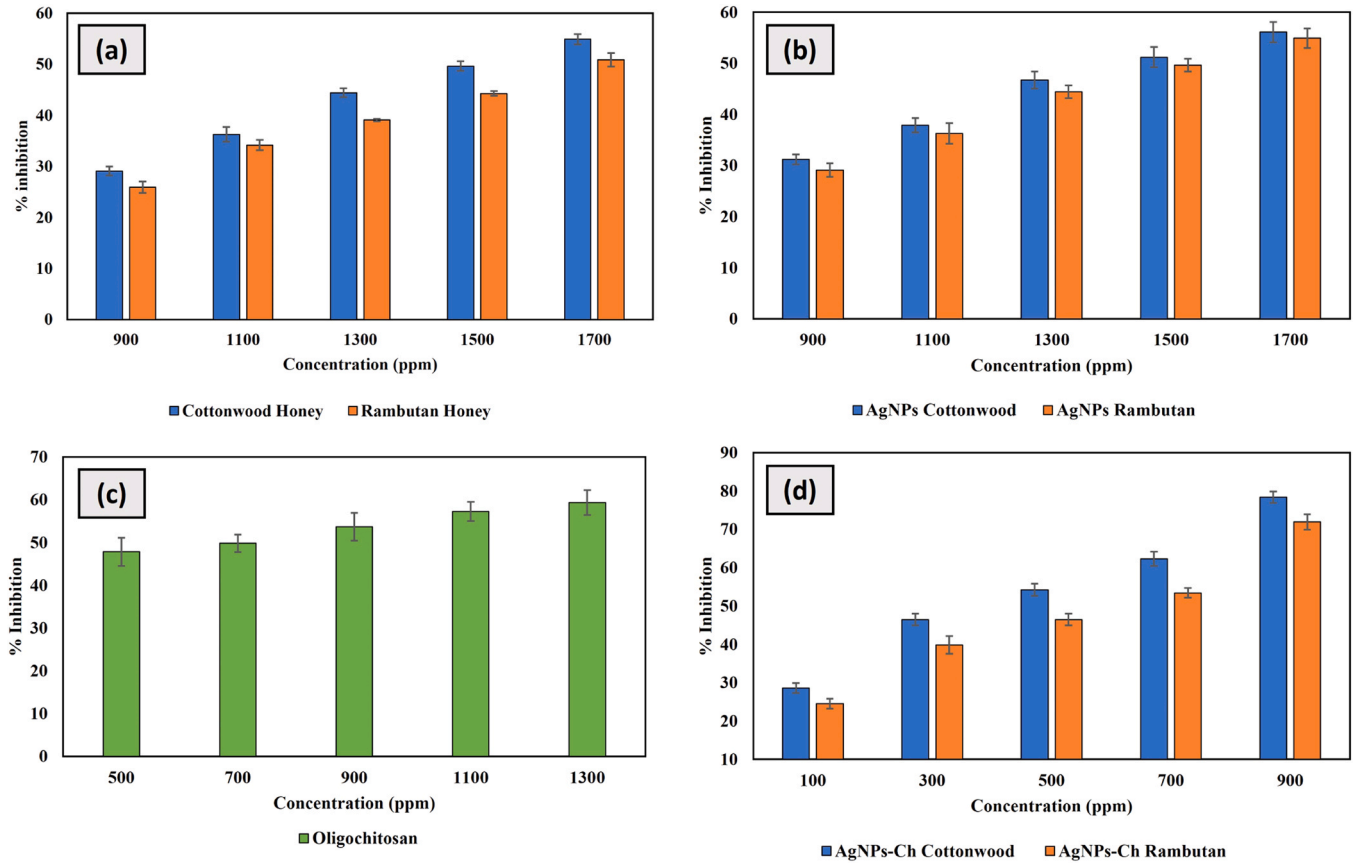

Fig. 14. Antioxidant activity (n = 3) of honey (a); AgNPs (b), Oligochitosan (c); and AgNPs-Ch (d).

Table 4
Antioxidant activity of honey, AgNPs, oligochitosan, and AgNPs-Ch.

Sample	IC_{50} µg/mL
Cottonwood Honey	$1519.53 \pm 4.11^{(b)}$
Rambutan Honey	$1662.09 \pm 8.30^{(c)}$
AgNPs Cottonwood	$1468.75 \pm 2.74^{(b)}$
AgNPs Rambutan	$1519.53 \pm 3.41^{(b)}$
Oligochitosan	$665.98 \pm 1.94^{(d)}$
AgNPs-Ch Cottonwood	$430.95 \pm 1.53^{(e)}$
AgNPs-Ch Rambutan	$551.29 \pm 5.09^{(e)}$

Note: The notation with different "letters" indicates a significant difference ($p < 0.05$).

The integration of polymeric stabilizers, particularly oligochitosan, has been demonstrated to significantly augment the antioxidant potential of AgNPs by improving colloidal stability, modulating electron transfer dynamics, and reducing aggregation-induced activity loss. Chitosan, a biocompatible polysaccharide, possesses intrinsic antioxidant properties attributed to its protonated amino groups, which facilitate radical scavenging. Furthermore, its ability to form electrostatic interactions with AgNPs not only reinforces nanoparticle stability but also modulates surface reactivity, thereby amplifying their ROS-neutralizing efficiency. Given the dependence of antioxidant mechanisms on nanoparticle size, charge distribution, and surface chemistry, chitosan-functionalized AgNPs may exhibit superior radical scavenging activity through synergistic effects between the metallic core and polymeric shell.

These findings underscore the necessity of post-synthetic modifications to tailor the bioactivity of AgNPs, particularly for applications where pristine nanoparticles exhibit suboptimal performance. The strategic incorporation of biocompatible polymeric coatings represents an advanced approach in nanomaterial engineering, enabling the fine-tuning of physicochemical properties to maximize therapeutic efficacy. This study thus highlights the pivotal role of polymer-functionalized AgNPs as an adaptive solution to enhance antioxidant potential, contributing to the broader development of nanotechnology-based biomedical interventions.

Firstly, oligochitosan is a natural biopolymer rich in amino (NH_2) and hydroxyl (-OH) groups, which possess inherent antioxidant properties. These functional groups can effectively scavenge free radicals and inhibit oxidative reactions. When chitosan coats the surface of AgNPs, its antioxidant activity synergizes with the plasmonic effects of the nanoparticles, amplifying their ability to interact with reactive oxygen species (ROS) or free radicals [58].

Secondly, oligochitosan acts as a biocompatible and stable nanocarrier. The chitosan coating enhances the colloidal stability of AgNPs, preventing aggregation and increasing the surface area available for interactions with free radicals. This stabilization enables AgNPs-Ch to more efficiently capture and neutralize free radicals compared to uncoated AgNPs [59,60].

Thirdly, oligochitosan serves as a nanoencapsulation agent, facilitating the controlled release of silver ions from the surface of AgNPs [61]. Silver ions are known to exhibit antioxidant activity through radical scavenging mechanisms, and their sustained release extends the duration of antioxidant activity in AgNPs-Ch. Furthermore, the nanoencapsulation effect of chitosan improves bioavailability and promotes active interactions between the nanoparticles and biological targets [62].

The synergistic combination of oligochitosan's intrinsic antioxidant properties, enhanced stability, and its role in controlled silver ion release contributes to the significant improvement in antioxidant activity observed in AgNPs-Ch. These findings underscore that chitosan coating not only enhances the physicochemical characteristics of AgNPs but also

amplifies their biological potential, particularly for antioxidant applications.

3.5. In vivo toxicity test

The toxicity assessment of AgNPs synthesized using honey bioreductors (AgNPs Cottonwood and AgNPs Rambutan) as well as their oligochitosan-coated counterparts (AgNPs-Ch Cottonwood and AgNPs-Ch Rambutan), reveals significant differences in larval shrimp toxicity, measured via LC_{50} values (Table 5). For uncoated AgNPs, the LC_{50} of AgNPs Rambutan was 417.53 ± 27.68 μg/mL, whereas AgNPs Cottonwood demonstrated a higher LC_{50} of 546.69 ± 22.21 μg/mL. This suggests that AgNPs synthesized using Rambutan honey exhibit higher toxicity toward shrimp larvae compared to those synthesized with Cottonwood honey. The difference in toxicity can be attributed to variations in the chemical composition of the two types of honey, which influence the size, morphology, and stability of the nanoparticles, ultimately affecting the release of silver ions and their corresponding toxicity.

The oligochitosan coating significantly increased the LC_{50} values for both nanoparticle samples, indicating a substantial reduction in toxicity. For the AgNPs-Ch Rambutan sample, the LC_{50} value increased to 2557.97 ± 23.06 μg/mL, while the AgNPs-Ch Cottonwood sample reached 3379.68 ± 20.00 μg/mL. These results reflect a marked decrease in toxicity, with reductions of 6.19-fold and 6.12-fold for AgNPs synthesized using cottonwood and rambutan honey, respectively. ANOVA revealed highly significant differences among the groups ($F = 55{,}192.57$, $p < 0.0001$), prompting further analysis via Tukey HSD.

Uncoated AgNPs exhibited the highest cytotoxicity, as evidenced by their markedly lower LC_{50} values (417.53–546.69 μg/mL, groups d-c). The significantly higher toxicity of AgNPs Rambutan relative to AgNPs Cottonwood ($p < 0.0001$) suggests that precursor composition influences nanoparticle toxicity, possibly due to differences in capping agents and surface charge distribution.

In stark contrast, chitosan-functionalized AgNPs (AgNPs-Ch) demonstrated a drastic reduction in cytotoxicity, with LC_{50} values increasing to 2557.97–3379.68 μg/mL ($p < 0.0001$, groups a-b). The significant elevation in LC_{50} underscores the biocompatibility enhancement conferred by chitosan, likely attributable to its well-documented role in stabilizing nanoparticle surfaces and mitigating oxidative stress-induced cytotoxicity.

Among AgNPs-Ch samples, AgNPs-Ch Cottonwood exhibited the highest LC_{50} (3379.68 μg/mL, group a), indicating superior biocompatibility. This suggests that variations in honey-mediated synthesis, possibly related to phytochemical composition and particle size distribution, may further modulate nanoparticle safety profiles. These findings strongly support the chitosan-mediated modulation of AgNP toxicity, positioning AgNPs-Ch as a promising candidate for biomedical applications requiring reduced cytotoxicity while preserving functional bioactivity.

This drastic improvement in biocompatibility highlights the effectiveness of oligochitosan as a coating agent in mitigating the release of silver ions, which are the primary contributors to AgNPs toxicity. Oligochitosan serves as a physical barrier, limiting nanoparticle interactions with biological cells, while its intrinsic antioxidant properties provide additional protection against oxidative stress induced by AgNPs. Comparative analysis of the samples reveals that, prior to oligochitosan coating, AgNPs Rambutan were more toxic than AgNPs Cottonwood. However, after oligochitosan coating, both types of nanoparticles exhibited significantly reduced toxicity, with AgNPs-Ch Cottonwood demonstrating greater biocompatibility than AgNPs-Ch Rambutan. These findings strongly support the role of chitosan in enhancing the safety profile of AgNPs, while also highlighting the influence of the bioreductant on the initial properties and toxicity of the nanoparticles before coating.

The oligochitosan coating plays a critical role by forming a protective layer around the AgNPs, effectively reducing the release of Ag^+ ions, which are known to be the main agents of AgNPs toxicity. Ag^+ ions exhibit high reactivity, causing damage to cellular membranes, proteins, and DNA within organisms, including shrimp larvae. The chitosan layer minimizes this ion release, thereby lowering the risk of biological damage.

Furthermore, oligochitosan's intrinsic biocompatibility enhances its protective effects. As a polycationic polymer, oligochitosan interacts gently with negatively charged cell membranes without causing significant harm. This property is crucial for mitigating the toxic impact typically associated with direct interactions between bare AgNPs and biological systems. In addition, chitosan has been shown to facilitate cellular regeneration and tissue healing, further reducing the toxic effects of nanoparticles.

The physicochemical stability of AgNPs is also enhanced by the chitosan coating, which prevents nanoparticle aggregation. The stabilization of particle size ensures more controlled biological interactions, reducing the potential for toxicity. Additionally, chitosan's antioxidant properties mitigate oxidative stress, a primary mechanism of cellular damage induced by AgNPs. By reducing oxidative stress, chitosan further contributes to the diminished toxicity of the nanoparticles. The chitosan coating not only improves the physicochemical stability and reduces the release of silver ions but also provides a protective mechanism against biological toxicity. These improvements render AgNPs

Table 5
Toxicity assessment of AgNPs and AgNPs-Ch conducted via the BSLT method.

Sample	Concentration (log)	Number of Surviving Nauplii (24 h)			Number of Nauplii Survivors ($\bar{x}$)	% Mortality ($\bar{x}$)	Probit ($\bar{x}$)	LC_{50}
		T1	T2	T3				
AgNPs Rambutan	0	9	8	8	8.33	16.67	4.03	417.53 ± 27.68$^{(d)}$
	1	8	7	7	7.33	26.67	4.37	
	2	6	7	5	6.00	40.00	4.75	
	3	5	4	4	4.33	56.67	5.16	
AgNPs	0	9	8	9	8.67	13.33	3.88	546.69 ± 22.21$^{(c)}$
Cottonwood	1	8	8	7	7.67	23.33	4.27	
	2	6	6	6	6.00	40.00	4.75	
	3	4	5	5	4.67	53.33	5.08	
AgNPs-Ch Rambutan	0	8	8	9	8.33	16.67	4.03	2557.97 ± 23.06$^{(b)}$
	1	7	8	9	8.00	20.00	4.17	
	2	7	7	6	6.67	33.33	4.57	
	3	5	6	5	5.33	46.67	4.91	
AgNPs-Ch	0	9	8	9	8.67	13.33	3.88	3379.68 ± 20.00$^{(a)}$
Cottonwood	1	8	8	8	8.00	20.00	4.17	
	2	7	7	8	7.33	26.67	4.37	
	3	5	6	5	5.33	46.67	4.91	

Note: The notation with different "letters" indicates a significant difference ($p < 0.05$).

safer and more biocompatible for biomedical and environmental applications, as evidenced by the larval shrimp toxicity tests.

3.6. Limitation and future perspectives

Despite the successful chitosan coating that significantly enhanced the biological performance of AgNPs, including antioxidant activity and reduced toxicity, the overall colloidal stability of the AgNPs remains a limitation. This is evidenced by the zeta potential values, which remain below the ± 30 mV threshold typically indicative of high nanoparticle stability. Although the chitosan layer contributed to improved dispersion and surface passivation, it was insufficient to achieve optimal electrostatic repulsion. This suggests that further surface engineering—either through the incorporation of alternative biocompatible polymers with stronger stabilizing capacity or by optimizing the synthesis conditions, such as irradiation parameters, concentration ratios, or pH environment—will be necessary to enhance nanoparticle stability. Achieving higher stability is crucial not only for ensuring long-term shelf life and uniformity but also for maximizing biological efficacy in downstream applications.

4. Conclusions

In this study, silver nanoparticles modified with oligochitosan (AgNPs-Ch) were successfully synthesized via a green approach using honey as a natural bioreductant. The primary objectives—to develop an environmentally friendly synthetic route and to investigate the effect of oligochitosan modification on the antioxidant potential of AgNPs—were effectively achieved. UV–Vis spectroscopy revealed a characteristic surface plasmon resonance peak at 430 nm, confirming the formation of AgNPs. While oligochitosan coating did not cause a significant shift in the absorption wavelength, FTIR analysis indicated strong interfacial interactions, particularly through hydroxyl and amine functional groups. TEM revealed uniformly spherical particles with an average diameter of approximately 9.01 nm, while SEM-EDX analysis confirmed the presence of silver as the dominant elemental constituent, along with carbon, nitrogen, and oxygen from oligochitosan acting as a stabilizing agent.

Antioxidant activity, evaluated using the DPPH assay, demonstrated that AgNPs-Ch exhibited significantly enhanced radical scavenging capacity compared to uncoated AgNPs, highlighting the synergistic effect of oligochitosan in augmenting the bioactivity of the nanomaterial. Moreover, the modification was shown to reduce nanoparticle toxicity while improving colloidal stability. Collectively, these findings position AgNPs-Ch as a promising candidate for antioxidant-based therapeutic applications, and contribute to the advancement of biocompatible and sustainable nanomaterials for biomedical use.

CRediT authorship contribution statement

Saidun Fiddaroini: Writing – review & editing, Writing – original draft, Visualization, Software, Investigation, Formal analysis, Analyzed and interpreted the data. Friske Prisilia, Silvana Br Karo: Investigation, Formal analysis. Luailik Madaniyah, Almas Dwi Khairana and Galuh Rahmaniah: Formal Analysis. Suci Amalia: Supervision, Investigation. Aulanni'am: conceived and designed the experiments, analyzed and interpreted the data. Moh. Farid Rahman: conceived and designed the experiments, wrote the manuscript Layta Dinira, Qonitah Fardiyah: Supervision. Akhmad Sabarudin: conceived and designed the experiments, analyzed and interpreted the data, contributed reagents, materials, analysis tools or data, wrote the manuscript.

Declaration of Generative AI and AI-assisted technologies in the writing process

During the preparation of this work, the authors used ChatGPT to enhance the readability of the English language.

Declaration of Competing Interest

The authors declare that they have no known competing financial interests or personal relationships that could have appeared to influence the work reported in this paper.

Acknowledgement

The authors would like to thank the Faculty of Science, Brawijaya University through the financial support through the Professorship Grant, with the number: 02172.6/UN10.F0901/B/KS/2024.

Data availability

All data related to this article are included in this paper

References

[1] S. Malik, K. Muhammad, Y. Waheed, Nanotechnology: a revolution in modern industry, Molecules 28 (2023) 661, https://doi.org/10.3390/molecules28020661.
[2] B. Elzein, Nano revolution: "tiny tech, big impact: how nanotechnology is driving SDGs progress", Heliyon 10 (2024) e31393, https://doi.org/10.1016/j.heliyon.2024.e31393.
[3] M. Taran, M. Safaei, N. Karimi, A. Almasi, Benefits and application of nanotechnology in environmental science: an overview, Biointerface Res Appl. Chem. 11 (2020) 7860–7870, https://doi.org/10.33263/BRIAC111.78607870.
[4] N.B. Singh, B. Kumar, U.L. Usman, Md.A.B.H. Susan, Nano revolution: exploring the frontiers of nanomaterials in science, technology, and society, Nano-Struct. Nano-Objects 39 (2024) 101299, https://doi.org/10.1016/j.nanoso.2024.101299.
[5] A. Dhaka, S. Chand Mali, S. Sharma, R. Trivedi, A review on biological synthesis of silver nanoparticles and their potential applications, Results Chem. 6 (2023) 101108, https://doi.org/10.1016/j.rechem.2023.101108.
[6] M. Fahim, A. Shahzaib, N. Nishat, A. Jahan, T.A. Bhat, A. Inam, Green synthesis of silver nanoparticles: A comprehensive review of methods, influencing factors, and applications, JCIS Open 16 (2024) 100125, https://doi.org/10.1016/j.jciso.2024.100125.
[7] R. Abbas, J. Luo, X. Qi, A. Naz, I.A. Khan, H. Liu, S. Yu, J. Wei, Silver nanoparticles: synthesis, structure, properties and applications, Nanomaterials 14 (2024) 1425, https://doi.org/10.3390/nano14171425.
[8] H.D. Beyene, A.A. Werkneh, H.K. Bezabh, T.G. Ambaye, Synthesis paradigm and applications of silver nanoparticles (AgNPs), a review, Sustain. Mater. Technol. 13 (2017) 18–23, https://doi.org/10.1016/j.susmat.2017.08.001.
[9] X.-F. Zhang, Z.-G. Liu, W. Shen, S. Gurunathan, Silver nanoparticles: synthesis, characterization, properties, applications, and therapeutic approaches, IJMS 17 (2016) 1534, https://doi.org/10.3390/ijms17091534.
[10] S. Fiddaroini, K. Indu, S. Amalia, I.O. Wulandari, A. Mulyasuryani, L. Dinira, A. Sabarudin, Cottonwood honey (Ceiba pentandra) as bioreductor for preparation of AgNPs-mediated Chitosan-based hand gel sanitizer, TJNPR 7 (2023), https://doi.org/10.26538/tjnpr/v7i12.29.
[11] S. Fiddaroini, K. Indu, L. Madaniyah, S. Amalia, Aulanni'am, MohF. Rahman, A. Sabarudin, Chitosan-Coated silver nanoparticles with various floral honey bioreductors: a promising nonalcoholic hand gel sanitizer formulation, OpenNano 21 (2025) 100228, https://doi.org/10.1016/j.onano.2024.100228.
[12] A.K. Keshari, R. Srivastava, P. Singh, V.B. Yadav, G. Nath, Antioxidant and antibacterial activity of silver nanoparticles synthesized by Cestrum nocturnum, J. Ayurveda Integr. Med. 11 (2020) 37–44, https://doi.org/10.1016/j.jaim.2017.11.003.
[13] Z. Zhangabay, D. Berillo, Antimicrobial and antioxidant activity of AgNPs stabilized with Calendula officinalis flower extract, Results Surf. Interfaces 11 (2023) 100109, https://doi.org/10.1016/j.rsurfi.2023.100109.
[14] R. Vishwanath, B. Negi, Conventional and green methods of synthesis of silver nanoparticles and their antimicrobial properties, Curr. Res. Green. Sustain. Chem. 4 (2021) 100205, https://doi.org/10.1016/j.crgsc.2021.100205.
[15] R.R. Bhosale, A.S. Kulkarni, S.S. Gilda, N.H. Aloorkar, R.A. Osmani, B.R. Harkare, Innovative eco-friendly approaches for green synthesis of silver nanoparticles, PCI-Approv. -IJPSN 7 (2014) 2328–2337, https://doi.org/10.37285/ijpsn.2014.7.1.3.
[16] L. Madaniyah, S. Fiddaroini, E.K. Hayati, MohF. Rahman, A. Sabarudin, Biosynthesis, characterization, and in-vitro anticancer effect of plant-mediated silver nanoparticles using Acalypha indica Linn: In-silico approach, OpenNano 21 (2025) 100220, https://doi.org/10.1016/j.onano.2024.100220.
[17] L. Madaniyah, S. Fiddaroini, E.K. Hayati, MohF. Rahman, A. Sabarudin, Stability of biologically synthesized silver nanoparticles (AgNPs) using Acalypha indica L. plant extract as bioreductor and their potential as anticancer agents against T47D cells, Sci. Technol. Indones. 10 (2025) 101–110, https://doi.org/10.26554/sti.2025.10.1.101-110.
[18] E. Abada, A. Mashraqi, Y. Modafer, M.A. Al Abboud, A. El-Shabasy, Review green synthesis of silver nanoparticles by using plant extracts and their antimicrobial

activity, Saudi J. Biol. Sci. 31 (2024) 103877, https://doi.org/10.1016/j.sjbs.2023.103877.
[19] N. Ahmad, M.A. Malik, A.H. Wani, M.Y. Bhat, Biogenic silver nanoparticles from fungal sources: Synthesis, characterization, and antifungal potential, Microb. Pathog. 193 (2024) 106742, https://doi.org/10.1016/j.micpath.2024.106742.
[20] K. Gudikandula, P. Vadapally, M.A. Singara Charya, Biogenic synthesis of silver nanoparticles from white rot fungi: their characterization and antibacterial studies, OpenNano 2 (2017) 64–78, https://doi.org/10.1016/j.onano.2017.07.002.
[21] C. Gasbarri, G. Angelini, Honey-assisted synthesis and properties of silver nanoparticles in aqueous solution and inside supramolecular aggregates. The Cassyopea® effect, Colloids Surf. A: Physicochem. Eng. Asp. 691 (2024) 133852, https://doi.org/10.1016/j.colsurfa.2024.133852.
[22] A. Muthu Kumara Pandian, B. Gopalakrishnan, M. Rajasimman, N. Rajamohan, C. Karthikeyan, Green synthesis of bio-functionalized nano-particles for the application of copper removal – characterization and modeling studies, Environ. Res. 197 (2021) 111140, https://doi.org/10.1016/j.envres.2021.111140.
[23] S. Mukherjee, A. Verma, L. Kong, A.K. Rengan, D.M. Cahill, Advancements in green nanoparticle technology: focusing on the treatment of clinical phytopathogens, Biomolecules 14 (2024) 1082, https://doi.org/10.3390/biom14091082.
[24] B. Olas, Honey and its phenolic compounds as an effective natural medicine for cardiovascular diseases in humans? Nutrients 12 (2020) 283, https://doi.org/10.3390/nu12020283.
[25] C. Rodríguez-Pólit, R. Gonzalez-Pastor, J. Heredia-Moya, S.E. Carrera-Pacheco, F. Castillo-Solis, R. Vallejo-Imbaquingo, C. Barba-Ostria, L.P. Guamán, Chemical properties and biological activity of bee pollen, Molecules 28 (2023) 7768, https://doi.org/10.3390/molecules28237768.
[26] S.A.M. Khalifa, A.A. Shetaia, N. Eid, A.A. Abd El-Wahed, T.Z. Abolibda, A. El Omri, Q. Yu, M.A. Shenashen, H. Hussain, M.F. Salem, Z. Guo, A.M. Alanazi, H.R. El-Seedi, Green innovation and synthesis of honeybee products-mediated nanoparticles: potential approaches and wide applications, Bioengineering 11 (2024) 829, https://doi.org/10.3390/bioengineering11080829.
[27] G. Czernel, D. Bloch, A. Matwijczuk, J. Cieśla, M. Kędzierska-Matysek, M. Florek, M. Gagoś, Biodirected synthesis of silver nanoparticles using aqueous honey solutions and evaluation of their antifungal activity against pathogenic Candida Spp, IJMS 22 (2021) 7715, https://doi.org/10.3390/ijms22147715.
[28] G.M. Shayo, E. Elimbinzi, G.N. Shao, Preparation methods, applications, toxicity and mechanisms of silver nanoparticles as bactericidal agent and superiority of green synthesis method, Heliyon 10 (2024) e36539, https://doi.org/10.1016/j.heliyon.2024.e36539.
[29] S.K. Mehta, S. Chaudhary, M. Gradzielski, Time dependence of nucleation and growth of silver nanoparticles generated by sugar reduction in micellar media, J. Colloid Interface Sci. 343 (2010) 447–453, https://doi.org/10.1016/j.jcis.2009.11.053.
[30] A. Dutta, A. Paul, A. Chattopadhyay, The effect of temperature on the aggregation kinetics of partially bare gold nanoparticles, RSC Adv. 6 (2016) 82138–82149, https://doi.org/10.1039/C6RA17561A.
[31] R. Veerasamy, T.Z. Xin, S. Gunasagaran, T.F.W. Xiang, E.F.C. Yang, N. Jeyakumar, S.A. Dhanaraj, Biosynthesis of silver nanoparticles using mangosteen leaf extract and evaluation of their antimicrobial activities, J. Saudi Chem. Soc. 15 (2011) 113–120, https://doi.org/10.1016/j.jscs.2010.06.004.
[32] A. Zuhrotun, D.J. Oktaviani, A.N. Hasanah, Biosynthesis of gold and silver nanoparticles using phytochemical compounds, Molecules 28 (2023) 3240, https://doi.org/10.3390/molecules28073240.
[33] N. Bahari, N. Hashim, K. Abdan, A. Md Akim, B. Maringgal, L. Al-Shdifat, Role of honey as a bifunctional reducing and capping/stabilizing agent: application for silver and zinc oxide Nanoparticles, Nanomaterials 13 (2023) 1244, https://doi.org/10.3390/nano13071244.
[34] N.P.U. Nguyen, N.T. Dang, L. Doan, T.T.H. Nguyen, Synthesis of silver nanoparticles: from conventional to 'modern' methods—a review, Processes 11 (2023) 2617, https://doi.org/10.3390/pr11092617.
[35] G.A. Filip, B. Moldovan, I. Baldea, D. Olteanu, R. Suharoschi, N. Decea, C. M. Cismaru, E. Gal, M. Cenariu, S. Clichici, L. David, UV-light mediated green synthesis of silver and gold nanoparticles using Cornelian cherry fruit extract and their comparative effects in experimental inflammation, J. Photochem. Photobiol. B: Biol. 191 (2019) 26–37, https://doi.org/10.1016/j.jphotobiol.2018.12.006.
[36] A.S. Kumar, G. Madhu, E. John, S.V. Kuttinarayanan, S.K. Nair, Optical and antimicrobial properties of silver nanoparticles synthesized via green route using honey, Green. Process. Synth. 9 (2020) 268–274, https://doi.org/10.1515/gps-2020-0029.
[37] S.N.S. Anis, W.C. Liew, A. Mohd Marsin, I.I. Muhamad, S.H. Teh, A.Z. Md Khudzari, Microwave-assisted green synthesis of silver nanoparticles using pineapple leaves waste, Clean. Eng. Technol. 15 (2023) 100660, https://doi.org/10.1016/j.clet.2023.100660.
[38] S. Lee, B.-H. Jun, Silver nanoparticles: synthesis and application for nanomedicine, IJMS 20 (2019) 865, https://doi.org/10.3390/ijms20040865.
[39] A. Kara, B. Özçelik, Green synthesis of Chitosan-coated silver nanoparticles (Ch-AgNPs): harnessing nature for sustainable and safe nanomaterial production, Osman. Korkut Ata Üniversitesi Fen. Bilim. EnstitüS. ü Derg. 7 (2024) 1319–1341, https://doi.org/10.47495/okufbed.1456350.
[40] Z. Bedlovičová, I. Strapáč, M. Baláž, A. Salayová, A brief overview on antioxidant activity determination of silver nanoparticles, Molecules 25 (2020) 3191, https://doi.org/10.3390/molecules25143191.
[41] E. Dilshad, M. Bibi, N.A. Sheikh, K.F. Tamrin, Q. Mansoor, Q. Maqbool, M. Nawaz, Synthesis of Functional silver nanoparticles and microparticles with modifiers and evaluation of their antimicrobial, anticancer, and antioxidant activity, JFB 11 (2020) 76, https://doi.org/10.3390/jfb11040076.
[42] S. Rajabi, A. Ramazani, M. Hamidi, T. Naji, Artemia salina as a model organism in toxicity assessment of nanoparticles, DARU J. Pharm. Sci. 23 (2015) 20, https://doi.org/10.1186/s40199-015-0105-x.
[43] S.K.D.P. Pinheiro, A.K.M. Lima, T.B.A.R. Miguel, A.G.S. Filho, O.P. Ferreira, M.D. S. Pontes, R. Grillo, E.D.C. Miguel, Assessing toxicity mechanism of silver nanoparticles by using brine shrimp (Artemia salina) as model, Chemosphere 347 (2024) 140673, https://doi.org/10.1016/j.chemosphere.2023.140673.
[44] Md.B. Uddin Rabbi, S. Haque, S. Bedoura, Advancements in synthesis, immobilization, characterization, and multifaceted applications of silver nanoparticles: a comprehensive review, Heliyon 10 (2024) e40931, https://doi.org/10.1016/j.heliyon.2024.e40931.
[45] S. Sysak, B. Czarczynska-Goslinska, P. Szyk, T. Koczorowski, D.T. Mlynarczyk, W. Szczolko, R. Lesyk, T. Goslinski, Metal nanoparticle-flavonoid connections: synthesis, physicochemical and biological properties, as well as potential applications in medicine, Nanomaterials 13 (2023) 1531, https://doi.org/10.3390/nano13091531.
[46] Y. Dai, Y. Guo, W. Tang, D. Chen, L. Xue, Y. Chen, Y. Guo, S. Wei, M. Wu, J. Dai, S. Wang, Reactive oxygen species-scavenging nanomaterials for the prevention and treatment of age-related diseases, J. Nanobiotechnol 22 (2024) 252, https://doi.org/10.1186/s12951-024-02501-9.
[47] B. Pucelik, A. Sułek, M. Borkowski, A. Barzowska, M. Kobielusz, J.M. Dąbrowski, Synthesis and characterization of size- and charge-tunable silver nanoparticles for selective anticancer and antibacterial treatment, ACS Appl. Mater. Interfaces 14 (2022) 14981–14996, https://doi.org/10.1021/acsami.2c01100.
[48] S. Varma, S. Dey, D. Palanisamy, Cellular uptake pathways of nanoparticles: process of endocytosis andfactors affecting their fate, CPB 23 (2022) 679–706, https://doi.org/10.2174/1389201022666210714145356.
[49] A. Ahmed Al-mehdhar, K. Mohammed Alarjani, N. Salem Aldosari, M. Ahmed Alghamdi, Antibacterial Efficacy of AgNPs synthesized from extract and Staphylococcus aureus Culture Supernatant, J. King Saud. Univ. - Sci. 36 (2024) 103464, https://doi.org/10.1016/j.jksus.2024.103464.
[50] S. Khan, Y. Rukayadi, A.H. Jaafar, N.H. Ahmad, Antibacterial potential of silver nanoparticles (SP-AgNPs) synthesized from Syzygium polyanthum (Wight) Walp. against selected foodborne pathogens, Heliyon 9 (2023) e22771, https://doi.org/10.1016/j.heliyon.2023.e22771.
[51] Z.H. Obaid, S.A. Juda, A.F. Kaizal, J. Mohammed Salman, Biosynthesis of silver nano particles (AgNPs) from blue green algae (Arthrospira platensis) and their anti-pathogenic applications, J. King Saud. Univ. - Sci. 36 (2024) 103264, https://doi.org/10.1016/j.jksus.2024.103264.
[52] A. Abdelgadir, M. Adnan, M. Patel, J. Saxena, M.J. Alam, M.M. Alshahrani, R. Singh, M. Sachidanandan, R. Badraoui, A.J. Siddiqui, Probiotic Lactobacillus salivarius mediated synthesis of silver nanoparticles (AgNPs-LS): a sustainable approach and multifaceted biomedical application, Heliyon 10 (2024) e37987, https://doi.org/10.1016/j.heliyon.2024.e37987.
[53] A. Dehnoee, R. Javad Kalbasi, M.M. Zangeneh, M. Delnavazi, A. Zangeneh, One-step synthesis of silver nanostructures using *Heracleum persicum* fruit extract, their cytotoxic activity, anti-cancer and anti-oxidant activities, Micro & Nano Lett. 18 (2023) e12153, https://doi.org/10.1049/mna2.12153.
[54] E. Pirabbasi, M.M. Zangeneh, A. Zangeneh, R. Moradi, M. Kalantar, Chemical characterization and effect of *Ziziphora clinopodioides* green-synthesized silver nanoparticles on cytotoxicity, antioxidant, and antidiabetic activities in streptozotocin-induced hepatotoxicity in Wistar diabetic male rats, Food Sci. Nutr. 12 (2024) 3443–3451, https://doi.org/10.1002/fsn3.4008.
[55] P. Moteriya, S. Chanda, Biosynthesis of silver nanoparticles formation from Caesalpinia pulcherrima stem metabolites and their broad spectrum biological activities, J. Genet. Eng. Biotechnol. 16 (2018) 105–113, https://doi.org/10.1016/j.jgeb.2017.12.003.
[56] H.I. Chiu, C.N.A. Che Mood, N.N. Mohamad Zain, M.R. Ramachandran, N. Yahaya, N.N.S. Nik Mohamed Kamal, W.H. Tung, Y.K. Yong, C.K. Lee, V. Lim, Biogenic silver nanoparticles of clinacanthus nutans as antioxidant with antimicrobial and cytotoxic effects, Bioinorg. Chem. Appl. 2021 (2021) 1–11, https://doi.org/10.1155/2021/9920890.
[57] J.K. Patra, K. Baek, Biosynthesis of silver nanoparticles using aqueous extract of silky hairs of corn and investigation of its antibacterial and anticandidal synergistic activity and antioxidant potential, IET Nanobiotechnol 10 (2016) 326–333, https://doi.org/10.1049/iet-nbt.2015.0102.
[58] Y. Herdiana, P. Husni, S. Nurhasanah, S. Shamsuddin, N. Wathoni, Chitosan-based nano systems for natural antioxidants in breast cancer therapy, Polymers 15 (2023) 2953, https://doi.org/10.3390/polym15132953.
[59] S.K. Dubey, T. Bhatt, M. Agrawal, R.N. Saha, S. Saraf, S. Saraf, A. Alexander, Application of chitosan modified nanocarriers in breast cancer, Int. J. Biol. Macromol. 194 (2022) 521–538, https://doi.org/10.1016/j.ijbiomac.2021.11.095.
[60] V. Mikušová, P. Mikuš, Advances in Chitosan-based nanoparticles for drug delivery, IJMS 22 (2021) 9652, https://doi.org/10.3390/ijms22179652.
[61] C. Krishnamoorthy, P. Chatterjee, U. Paul, S. Banerjee, L. Kumar, R. Chidambaram, Nanoencapsulation of antimicrobial agents and antimicrobial effect of silver nanoparticles. in: Nanotechnology Applications for Food Safety and Quality Monitoring, Elsevier, 2023, pp. 435–456, https://doi.org/10.1016/B978-0-323-85791-8.00023-9.
[62] S.S. Behera, A.G. Majumdar, H. Gullani, A.L. Roy, A.K. Dash, P.K. Behera, Z. Parwez, S. Giri, P.S. Mohanty, L. Ray, Green synthesis of silver-chitosan nanocomposite exhibits promising antibiofilm properties against pathogenic bacteria Escherichia coli and Staphylococcus aureus, Microbe 6 (2025) 100264, https://doi.org/10.1016/j.microb.2025.100264.